AgriEngineering

MDPI

Article

Phenological Monitoring of Irrigated Sugarcane Using Google Earth Engine, Time Series, and TIMESAT in the Brazilian Semi-Arid

Diego Rosyur Castro Manrique [1], Pabrício Marcos Oliveira Lopes [1,*], Cristina Rodrigues Nascimento [1], Eberson Pessoa Ribeiro [2] and Anderson Santos da Silva [3]

[1] Departament of Agronomy, Federal Rural University of Pernambuco (UFRPE), Street Dom Manoel de Medeiros, s/nº, Dois Irmaos, Recife 52171-900, Pernambuco, Brazil; dicroud@gmail.com (D.R.C.M.); cristina.nascimento@ufrpe.br (C.R.N.)

[2] Federal Institute of Pernambuco, Avenue Professor Luiz Freire, Recife 50740-545, Pernambuco, Brazil; eberson_pessoa@yahoo.com.br

[3] Department of Agronomy, Federal University of Agreste of Pernambuco, Garanhuns 55292-278, Pernambuco, Brazil; anderson.silva@ufape.edu.br

* Correspondence: pabricio.lopes@ufrpe.br or pabriciope@gmail.com

Abstract: Monitoring sugarcane phenology is essential since the globalized market requires reliable information on the quantity of raw materials for the industrial production of sugar and alcohol. In this context, the general objective of this study was to evaluate the phenological seasonality of the sugarcane varieties SP 79-1011 and VAP 90-212 observed from the NDVI time series over 19 years (2001–2020) from global databases. In addition, this research had the following specific objectives: (i) to estimate phenological parameters (Start of Season (SOS), End of Season (EOS), Length of Season (LOS), and Peak of Season (POS)) using TIMESAT software in version 3.3 applied to the NDVI time series over 19 years; (ii) to characterize the land use and land cover obtained from the MapBiomas project; (iii) to analyze rainfall variability; and (iv) to validate the sugarcane harvest date (SP 79-1011). This study was carried out in sugarcane growing areas in Juazeiro, Bahia, Brazil. The results showed that the NDVI time series did not follow the rainfall in the region. The sugarcane areas advanced over the savanna formation (Caatinga), reducing them to remnants along the irrigation channels. The comparison of the observed harvest dates of the SP 79-1011 variety to the values estimated with the TIMESAT software showed an excellent fit of 0.99. The mean absolute error in estimating the sugarcane harvest date was approximately ten days, with a performance index of 0.99 and a correlation coefficient of 0.99, significant at a 5% confidence level. The TIMESAT software was able to estimate the phenological parameters of sugarcane using MODIS sensor images processed on the Google Earth Engine platform during the evaluated period (2001 to 2020).

Keywords: MODIS; NDVI; harvest; MapBiomas; rainfall

check for updates

Citation: Castro Manrique, D.R.; Lopes, P.M.O.; Nascimento, C.R.; Ribeiro, E.P.; Silva, A.S.d. Phenological Monitoring of Irrigated Sugarcane Using Google Earth Engine, Time Series, and TIMESAT in the Brazilian Semi-Arid. *AgriEngineering* **2024**, *6*, 3799–3822. https://doi.org/10.3390/agriengineering6040217

Academic Editors: Fatwa Ramdani, Riswan S. Sianturi and Adi Wibowo

Received: 1 July 2024
Revised: 26 September 2024
Accepted: 26 September 2024
Published: 18 October 2024

Copyright: © 2024 by the authors. Licensee MDPI, Basel, Switzerland. This article is an open access article distributed under the terms and conditions of the Creative Commons Attribution (CC BY) license (https://creativecommons.org/licenses/by/4.0/).

1. Introduction

Sugarcane (*Saccharum* spp. L., plant C4) is a cultural product of great social, economic, and environmental importance, with Brazil as the largest producer in the world, followed by India and China, due to its edaphoclimatic conditions and widely cultivated areas [1–3]. As the global demand for energy increases, sugarcane has also been planted in regions where drought is frequent, contributing to an 8% increase in electric energy production from biomass thermal plants, reaching 2588 GWh (Gigawatt hour) in the first quarter of 2024 [4,5]. Especially in the Northeast Region of Brazil, production is expected to increase by 4.7%, totaling 59.55 million tons, influenced mainly by an increase in cultivated areas, while productivity remains stable [6]. In Juazeiro, Bahia, the area planted with sugarcane measures 17,500 hectares, with expectations for the 2023 harvest to produce 1.9 million tons

of sugarcane, transformed into 150 thousand tons of sugar, 56 million liters of ethanol, and generating 50 MW of energy [7].

In this context, remote sensing and the use of orbital images are fundamental to identifying and monitoring the culture cycle, allowing the mapping of cultivated areas, monitoring cultures, and evaluating alterations [8,9]. Sugarcane, a semi-perennial crop, presents a distinct spectral signature throughout its life cycle, facilitating its identification [10,11]. When analyzing agricultural images, the historical harvest calendars must be considered, given that different cultures are in varying stages of growth [12]. Studies developed tools to extract information on Earth Surface Phenology (PSL) from orbital data, making it possible to evaluate phenological behavior on a regional or continental scale and create data banks that help predict measurements and simulations on the influence of climate and Prague [13–20]. Therefore, analyzing the phenology of areas cultivated with sugarcane is crucial to understanding and monitoring the cultivation conditions and the carbon cycle [21].

The growth and development of the sugarcane grown in the Brazilian semi-arid region requires 1500 to 2500 mm according to the phenological phase to obtain optimal water conversion [22]. In 2022, around 28 million inhabitants lived in this region, divided into urban (62%) and rural (38%) areas. In livestock farming, cattle are the main animals, representing approximately 58.1% of the herds in the Northeast, dependent on these waters to survive [23]. The rational use of water is necessary to guarantee water for irrigation [24] and optimize productivity by replacing crops, especially to meet the demand for extensive livestock farming [25].

The annual crop calendar is imperative to rational water use, as it represents the crop cycle grown in harmony with the regional climate, local practices, and economic incentives. Therefore, each farmer adopts a specific sequence of preparing the field, planting, and harvesting to minimize labor and risk and maximize production [12]. For sugarcane industries, it is imperative not only to monitor the growth of the crop to predict the yield but also to obtain updates on the harvest progress throughout the harvest season to optimize the production processes [26]. However, many farmers use their technical experience to visually estimate sugarcane areas based on the vegetative vigor of the plantation. Based on information from previous harvests, farmers randomly estimate the productivity of sugarcane areas [27,28]. In addition, sugarcane harvest dates are established primarily through direct conversations with farmers [29]. However, it is difficult to maintain the inference method over large areas, which often generates biased data that do not reflect the actual productivity of crops [30]. The capability of automatically retrieving such information becomes a great asset [29].

Several software programs can estimate phenological metrics from satellite image time series, for example, CropPhenology in version 1.0 [31], phoenix in version 1.6 [32], phenolic in version 1.4-5 [33], greenbrown in version 2.2 [34], and Digital Earth Australia tools (DEA) in version 2.0 [35] in Python, among them the TIMESAT [36–39]. The TIMESAT is one of the most widely used software for analyzing time series of satellite images, especially in crop phenology studies [40]. Its effectiveness in estimating phenological metrics, such as harvest dates, is attributed to its ability to smooth noisy data, model seasonal patterns, and provide accurate estimates of plant development [36,39]. Among the main biophysical parameters used as input in the TIMESAT software, the Normalized Difference Vegetation Index (NDVI) stands out. This index is essential for capturing seasonal and interannual variations in vegetation conditions and environmental characteristics [41–44].

The time-series NDVI from the MOD13Q1 derived from the MODIS (Moderate-Resolution Imaging Spectroradiometer) provided an improved temporal resolution (images diary) and moderate spatial resolution (250, 500, and 1000 m), covering the globe with scientifically reliable spatial data sources [45]. It has rigorous validation with enhanced satellite products [46] and assists in extracting information from time series essential for research on ecosystem conditions [45]. The MOD13Q1 images are available on the Google Earth Engine (GEE) platform, which allows access to the free processing with considerable

time series to monitor the phenology of crops and facilitates the estimates of biophysical parameters [47].

The TIMESAT software estimates the early, middle, and end of the annual cycle of sugarcane, active vegetation accumulation, and total vegetation production, among others [36,48–50]. The end of the vegetative cycle or harvest date is imperative, as it will help with harvest planning and management [51], pest and disease control [52], and market forecasting [53], guaranteeing more efficient, sustainable, and profitable production for rural producers in the Brazilian semi-arid region. When estimating the harvest date for irrigated sugarcane, producers need to take into account the availability and distribution of rainfall in local areas, which can directly influence the sugarcane maturation process [54], sucrose content [55], and consequently, the ideal date for harvesting. Phenological monitoring of sugarcane in the semi-arid region is essential to assisting with productivity and guaranteeing the sustainability of culture in a region with significant climatic challenges.

Given the above reasons, this study aimed to evaluate the phenological seasonality of sugarcane observed from the NDVI time series over 19 years (2001–2020) from global databases. This study has four specific objectives: (i) estimate phenological parameters using a time series of NDVI over 19 years, (ii) characterize land use and land cover obtained from the MapBiomas project, (iii) analyze the variability of rainfall, and (iv) validate the harvest date of irrigated sugarcane in the Brazilian semi-arid region.

2. Material and Methods

2.1. Study Area

This study covers a portion of a commercial area cultivated with 100% irrigated sugarcane in the São Francisco valley. The study area is located in geographic coordinates between parallels 9°20′ S and 9°40′ S latitude and between meridians 40°13′ W and 40°0′ W longitude and an altitude of approximately 396 m above sea level (masl) in the municipality of Juazeiro-Bahia, Brazil (Figure 1).

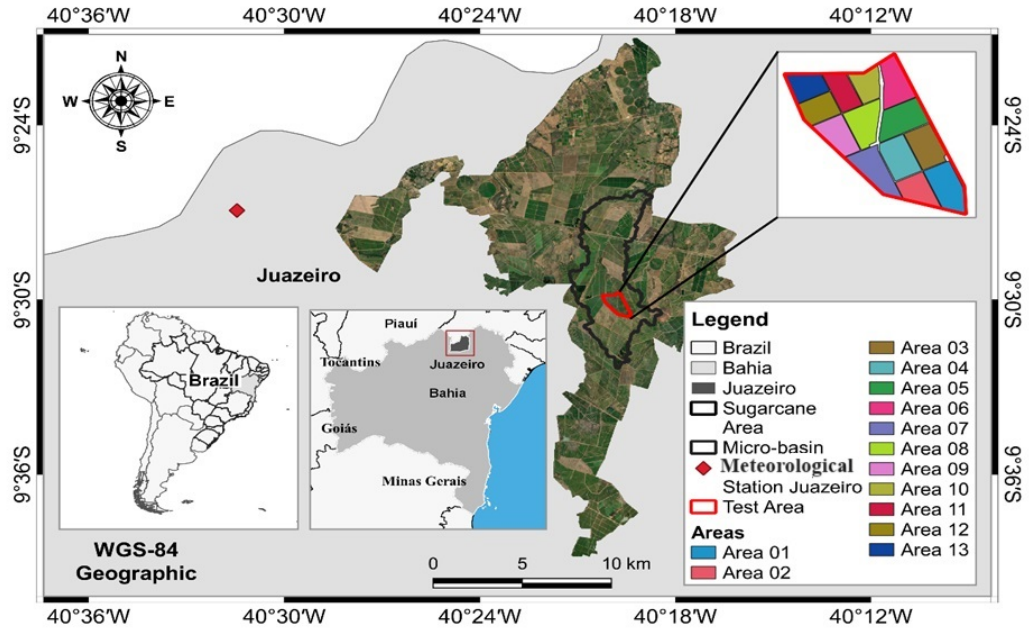

Figure 1. Map of the sugarcane with the physical boundaries in RGB (red, green and blue) color composite Landsat-8 and the location under study.

Koppen classifies the climate of the region in BSh [56] as hot semi-arid, with accumulated rainfall below 600 mm and an average air temperature of 25 °C to 30 °C throughout the year [57]. However, seasonally, the average annual rainfall varies widely from 300 mm to 1000 mm annually, mainly concentrated in 3 to 4 months during summer and autumn,

followed by a prolonged dry season lasting 8 to 9 months during winter and spring [58]. The region presents high interannual variability in rainfall, with long-lasting droughts and high potential evapotranspiration rates between 1500 mm and 2000 mm annually [59].

The study area is contained in the São Francisco River basin, having water potential, but there is no excess water in the soil, which imposes the need for additional irrigation. This farm has a cultivated area of approximately 20,000 hectares of sugarcane, the main variety grown being *Saccharum officinarum* ssp. [60]. The study area has 131.06 hectares (ha), of which 121.50 ha are planted with sugarcane, divided into 13 smaller areas, ranging from 6.88 to 11.64 ha, plus 0.22 ha are of stones and 9.34 ha are of streets and drains.

The study area presents soil the same: soil type (vertisol), a drip irrigation system, spacing (0.90 m × 2.10 m), a cultivated variety (SP 79-1011), and the type of harvest (manual). From the 2014 harvests, after planting renewal in the field, 93% of the area was filled by the VAT 90-212 variety, and the remaining 7% was composed of several other varieties [30].

The topography is flat and undulated with open valleys, where the predominant vegetation is a dense shrubby Caatinga that develops with greater vigor after the first signs of rainfall [61].

Table 1 presents information on sugarcane in the study area, from the first harvest in 1998 to the last in 2017. The renewal of planting with the VAT 90-212 variety occurred in the 2012/2013 crop year, with the first harvest in 2013/2014 and the second in 2014/2015. Information from 2018 to 2020 was not made available by the producer due to the termination of the contract between the university and the producer.

Table 1. Information on sugarcane of the study area for the crop years 1998 to 2017.

Crop Year	Varieties	Harvest	Harvest Season	Productivity (t.ha^{-1})
1998/1999	SP 79-1011	1st	-	146.00
1999/2000	SP 79-1011	2nd	-	105.00
2000/2001	SP 79-1011	3rd	-	113.00
2001/2002	SP 79-1011	4th	-	101.00
2002/2003	SP 79-1011	5th	-	117.00
2003/2004	SP 79-1011	6th	-	93.00
2004/2005	SP 79-1011	7th	November/2005	98.00
2005/2006 ^{PV}	SP 79-1011	8th	October/2008	101.51
2006/2007 ^{PV}	SP 79-1011	9th	October/2008	113.20
2007/2008 ^{PV}	SP 79-1011	10th	October/2008	96.20
2008/2009 ^{PV}	SP 79-1011	11th	September/2009	82.73
2009/2010 ^{PV}	SP 79-1011	12th	September/2010	83.36
2010/2011 ^{PV}	SP 79-1011	13th	August/2011	84.48
2011/2012 ^{PV}	SP 79-1011	14th	July/2012	74.28
2012/2013	-	-	Planting renewal	-
2013/2014	VAT 90-212	1st	June/2014	261.86
2014/2015	VAT 90-212	2nd	July/2015	171.77
2015/2016	VAT 90-212	3rd	July/2016	156.03
2016/2017	VAT 90-212	4th	July/2017	148.83

PV = Validation period of the TIMESAT software in version 3.3. Source: adapted of [28,30].

2.2. Sugarcane Harvest Dates in the Test Area

The actual sugarcane harvest dates took place in different months between 2006 and 2012 for the test area containing the 13 plots (Figure 1). The sugarcane harvest date was only validated for the SP-79-1011 variety from 2006 to 2012. The harvest data for the 2014 to 2017 crops were not made available by the company.

The sugarcane was harvested in October and November from 2006 to 2008, while from 2007 to 2012, the sugarcane was harvested in July, August, September, or October (Table 1).

Comparing the actual sugarcane harvest dates with those estimated by TIMESAT software [36] determines how many days the estimated dates differ from the actual sugar cane harvest dates.

2.3. Orbital Data

The MOD13Q1 Version 6.1 product provides an NDVI value on a per-pixel basis. The MODIS NDVI product undergoes a calculation of atmospherically corrected bidirectional surface reflectances and filters for water, clouds, heavy aerosols, and cloud shadows. A test checks the quality of the pixels and classifies them as pure pixels, receiving a value of zero. The MOD13Q1 product uses the maximum value composite (MVC) approach applied to MODIS imagery with a 16-day spatial resolution and 16-bit radiometric resolution (https://lpdaac.usgs.gov/, accessed on 1 January 2021). For the temporal study, 460 NDVI images of the product MOD13Q1 were used with a spatial resolution of 250 m and composition 16 days approaching the rectangle h14v09, referring to the years 2001 to 2020, from the MODIS sensor, aboard the Terra satellite. Therefore, the global MODIS NDVI monitoring data have a spatial resolution compatible with the size of sugarcane fields.

The MODIS NDVI images were made available by the National Aeronautics and Space Administration (NASA) website at the Land Processes Distributed Active Archive Center (LP DAAC), USGS/Earth Resources Observation and Science (EROS) Center, Sioux Falls, South Dakota (https://lpdaac.usgs.gov/, accessed on 30 January 2022), where they were cloud processed using the Google Earth Engine (GEE) Code platform.

The annual maps (2006 to 2012) of land cover and use classification derived from images from the Thematic Mapper (TM) sensor on board the LANDSAT-5 satellite were processed and made available on the Annual Mapping of Land Cover and Land Use in Brazil Project (MapBiomas). The classification is crucial for characterizing the study area made available in the cloud through the MapBiomas website (https://mapbiomas.org/, accessed on 1 june 2021) and processed on the Google Earth Engine Code platform.

2.4. Meteorological Data

The analysis of monthly data on accumulated rainfall (mm), total global solar radiation (MJ m^{-2}), average air temperature (°C), and average relative humidity (%) serves to verify the meteorological conditions of the study area in the years studied. However, the time series of meteorological data comprised only the period from 2008 to 2020 due to a lack of maintenance and previous measurements. These data were obtained from the automatic weather station of the Meteorology Laboratory (Labmet) of the Federal University of São Francisco Valley (UNIVASF), located in the municipality of Juazeiro, Bahia, Brazil (09°04′08″ S; 40°19′11″ W; and altitude of 387 m) (http://labmet.univasf.edu.br/, accessed on 1 June 2023).

2.5. TIMESAT Software

The phenological metrics represent the characteristics of the vegetation within its phenological cycle, or phenophases, corresponding to dimensionless output parameters and can be calculated based on the NDVI time series [62]. In this study, the TIMESAT software [54–56] was used to analyze 19 years of NDVI time series (from 2001 to 2020) and to compute phenological metrics: Start of Season (SOS), End Of Season (EOS), Length of the Season (LOS), and Peak of Season (POS), among others.

Figure 2 illustrates the energy source (Sun), the reflected energy from sugarcane, the satellite image capture, and the NDVI time series processing modules of the MOD13Q1 product in GEE and TIMESAT. In the Code Editor module of GEE, computational codes written in Javascript produce the time series of NDVI images of the MOD13Q1 product for the study area. The NDVI time series are then imported into TIMESAT software to estimate the phenological parameters of sugarcane. TIMESAT software estimates the Start of the Season (SOS), End Of Season (EOS), Length of the Season (LOS), and Peak of Season (POS), among other things.

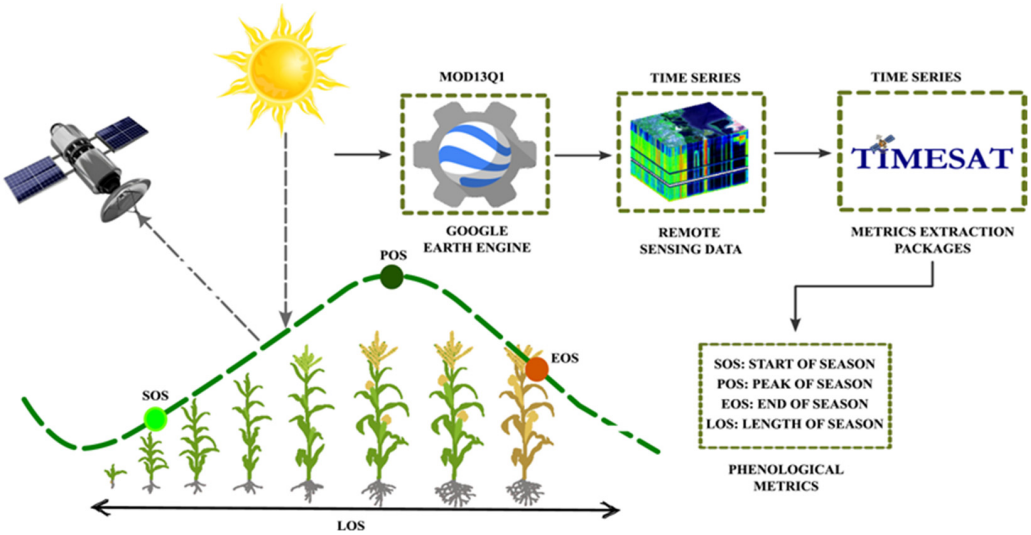

Figure 2. Graphical abstract steps for obtaining the phenological metrics. where: SOS = Start of Season, EOS = End Of Season, LOS = Length of the Season and POS = Peak of Season. Source: Adapted of Rodigheri et al. [40].

Figure 3 illustrates the processing stages of the TIMESAT software for obtaining phenological metrics from the NDVI time series. The TIMESAT software operates through a graphical user interface in Matrix Laboratory (MATLAB) software in the version 8.2. Stage 1 consists of preparing the NDVI time series. In this step, NDVI data from 2001 to 2020 in comma-separated values (CSV) format are converted to ASCII format and visualized in the TIMESAT IMAGE VIEW module.

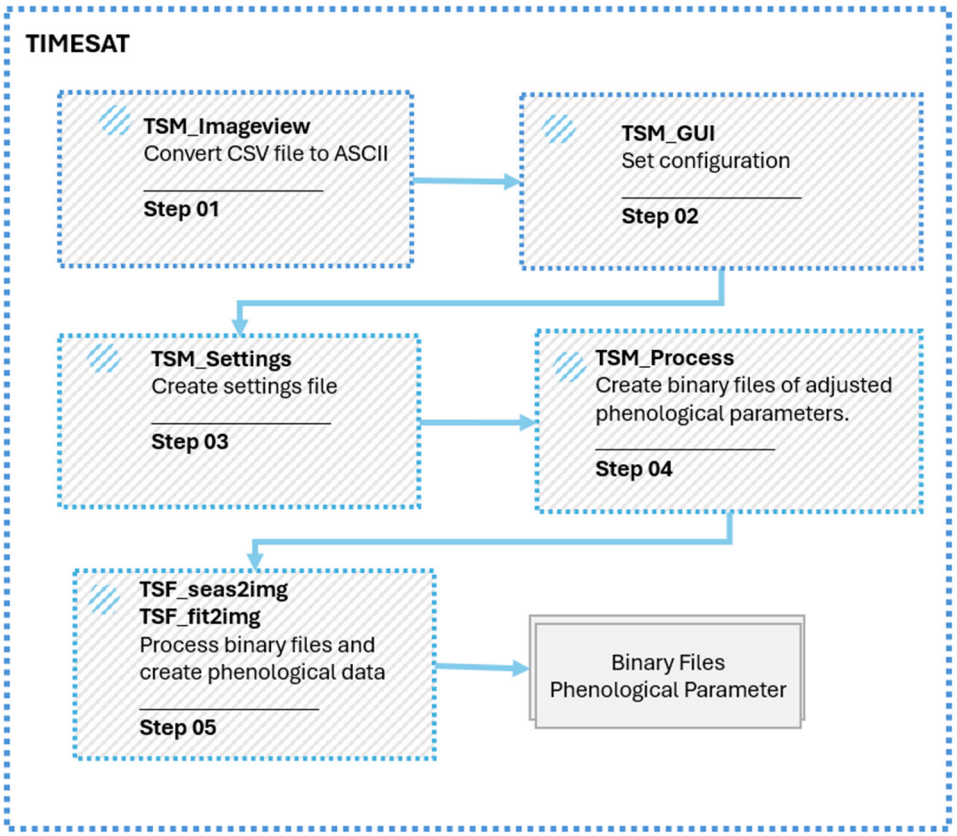

Figure 3. TIMESAT software modules for processing NDVI time series in the TIMESAT software module.

In step 2, the TIMESAT TSM GUI module checks the quality of the NDVI data file in ASCII format produced in step 1. This module also provides four data-fitting models for NDVI: Savitsky–Golay, Gaussian, or duplicate logistics. This study used the Savitsky–Golay model [63] because the NDVI time series adequately fit the fitting curve, minimizing the noise in the NDVI time series caused by clouds. The process of fitting the NDVI time series with the Savitsky–Golay model is in steps: (1) defining the number of phenological cycles and the number of years of the NDVI time series; (2) filtering NDVI data and fitting smoothing functions (Savitsky–Golay filter or asymmetric Gaussian functions fitted by least squares or double logistic smooth functions); and (3) estimating seasonality parameters.

In step 3, the TSM_settings module creates a file with settings in ASCII format. This file allows TIMESAT software to control the settings of the pixels and the land use and land cover classes.

In step 4, the Fortran TSF_process module uses the configuration file created in step 3, producing binary files of adjusted phenological parameters. These files contain the results of the input NDVI time series.

In step 5, the TSF_seas2img and TSF_fit2img module processes the binary files and produces the phenological parameter data. This TIMESAT software module also displays the phenological data per pixel at the set time.

Table 2 shows the input settings used in the TIMESAT software for the present study. Season start and end values of 0.2 are commonly used to represent a phenological cycle with an initial and final level of 20% of the seasonal range [62,64–67].

Figure 4 exemplifies the use of the Savitsky–Golay filter (red curve) for a time series of NDVI scaled as a function of time in days. The fitting curve no longer shows the noise of the NDVI time series (black curve). In the curve fitted with the Savitsky–Golay filter, points (a) and (b) mark the start and end of the season, respectively, points (c) and (d) give the 80% levels, (e) displays the point with the maximum value, (f) displays the seasonal amplitude, and (g) the seasonal length. Finally, (h) and (i) are integrals showing the cumulative effect of vegetation during the season [48–50].

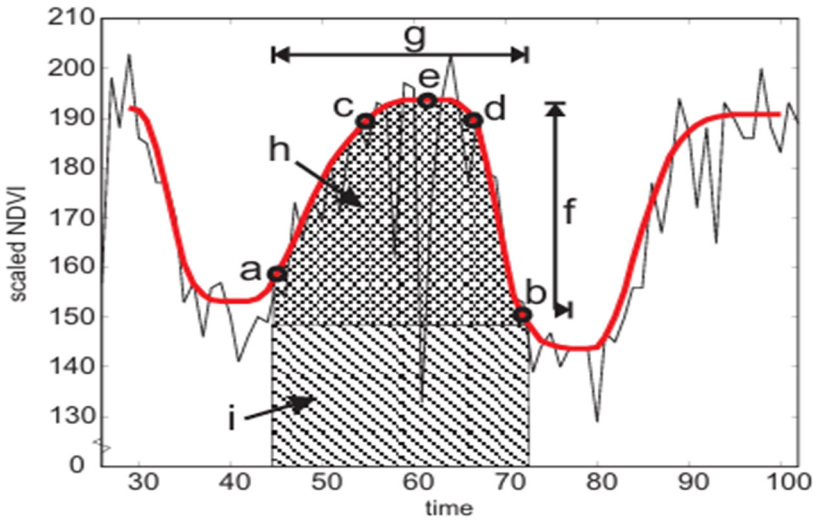

Figure 4. Application of the Savitsky–Golay filter (red curve) for a time series of NDVI scaled (black curve) as a function of time (days) to estimate phenological parameters: points (a) and (b) mark, respectively, start and end of the season, points (c) and (d) give the 80% levels, (e) displays the point with the maximum value, (f) displays the seasonal amplitude, (g) the seasonal length, and (h) and (i) are integrals showing the cumulative effect of vegetation during the season. Source: Jönsson and Eklundh [48].

Table 2. Input settings used in the TIMESAT software for the study area.

Configuration	Values
Seasonal par. (0–1)	1 (yes)
No. of iterations	2
Force Minimum Value	0 (no)
Adjustment method	Savitsky–Golay
Seasonal Amplitude	Seasonal Amplitude
Season start value	0.2
End-of-season value	0.2

2.6. Statistical Analysis and Validation of the Data

In this study, the Shapiro–Wilk normality test verified whether the harvest dates for the 13 plots of sugarcane followed a normal distribution, taking into account that the samples evaluated were less than 50 and greater than 3 [68], considering the following hypotheses: H0 (null): sugarcane harvest dates follow a normal distribution; H1 (alternative): Sugarcane harvest dates do not follow a normal distribution.

A Student's parametric *t*-test [69] checked, using Microsoft Excel software in the version 365, the acceptance of the H0 that the actual and estimated sugarcane harvest dates have equal means. If this condition is not satisfied, the H1 is accepted, considering that the averages differ from the observed and estimated harvest dates at the 5% significance level (*p*-value> 0.05).

Descriptive statistics of the actual harvest dates and estimates of the TIMESAT software were calculated by Microsoft Excel software and imported into the free QGIS software in the version 3.1 [70] to identify the variations in the collected data sets.

In addition, the accumulated monthly rainfall data measured at the UNIVASF automatic weather station partially explain the influence of rainfall on sugarcane harvest dates observed in the NDVI time series. However, the phenological parameters obtained by the TIMESAT software were compared to each other to determine the correlation coefficient and the tendency to increase or decrease between variables.

The comparison between the sugarcane harvest dates performed by the farm with those harvest dates estimated by the TIMESAT software for the period from 2006 to 2012 using the following statistical parameters:

Pearson Correlation (r) according to Equation (1) [71]:

$$r = \frac{\sum_{i=1}^{N}\left(Y_{obsi} - \overline{Y_{obsi}}\right)\left(Y_{esti} - \overline{Y_{esti}}\right)}{\sqrt{\sum_{i=1}^{N}\left(Y_{obsi} - \overline{Y_{obsi}}\right)^2}\sqrt{\sum_{i=1}^{N}\left(Y_{esti} - \overline{Y_{esti}}\right)^2}} \quad (1)$$

where: Y_{esti} is the estimated variable; Y_{obsi} is the observed variable; and N is the number of observations (i = 1, 2, . . ., n).

The adjusted coefficient of determination (adjusted R^2) according to Equation (2) [72]:

$$R^2_{Adjusted} = \left[1 - \frac{\left(1 - R^2\right)(N-1)}{N - K - 1}\right] \quad (2)$$

where: N is the number of observations (i = 1, 2, . . ., n), and K is the number of independent variables in the regression.

The root mean square error ($RMSE$) represented by Equation (3) [73]:

$$RMSE = \sqrt{\frac{\sum_{i=1}^{N}\left(Y_{obsi} - \overline{Y_{esti}}\right)^2}{N}} \quad (3)$$

The mean absolute error (*MAE*) illustrated in Equation (4) [73]:

$$MAE = \frac{\sum_{I=1}^{N} |Y_{obsi} - Y_{esti}|}{N} \quad (4)$$

where Y_{obsi} is the observed variable; Y_{esti} is the estimated variable; and N is the number of observations (i = 1, 2, . . ., n).

Willmott's concordance index (d) described by Equation (5) [74]:

$$d = 1 - \frac{\sum_{i=1}^{N} (Y_{esti} - Y_{obsi})^2}{\sum_{i=1}^{N} \left[\left| Y_{esti} - \overline{Y_{esti}} \right| + \left| Y_{obsi} - \overline{Y_{obsi}} \right| \right]} \quad (5)$$

where: Y_i is the estimated value; Y_{obsi} is the observed value; and $\overline{Y_{obsi}}$ and $\overline{Y_{esti}}$ are the averages of the observed and estimated values. Camargo and Sentelhas [75] developed the performance index (e) expressed by Equation (6):

$$e = r * d \quad (6)$$

where: r is Pearson's correlation coefficient; and d is Willmott's concordance index (1981).

Table 3 shows the values of the correlation coefficient (r) expressed by Camargo and Sentelhas [75] and the performance index (e) for the classification of the models expressed by Cohen [73]:

Table 3. Classification of the correlation coefficient (r) and the performance index (e) [75].

r	Performance r	e	Performance e
>0.9	Almost perfect	>0.85	Great
0.7–0.9	Very high	0.76–0.85	Very Good
0.5–0,7	High	0.66–0,75	Good
0.3–0.5	Moderate	0.61–0.65	Average
0.1–0.3	Low	0.51–0.60	Passable
0–0.1	Very low	0.41–0.50	Bad
-	-		Terrible

3. Results

3.1. Time Series of Meteorological Data

Figure 5 shows the variability of monthly air temperature, cumulative rainfall (mm), global radiation (MJ m^{-2}), and relative humidity (%) from the Meteorology Laboratory (Labmet) automatic weather station at UNIVASF for the available period between 2008 and 2020. In 2016, the highest rainfall records occurred. The dry and rainy periods are more frequent between May to October and November to April, respectively, except for 2011, when the accumulated rainfall between December and February reached 126 mm $month^{-1}$.

The air temperature ranged from 23.3 °C to 30.5 °C, with the highest air temperature records occurring in 2013 and 2015, in March and November, respectively, and the lowest air temperatures occurred in 2008 and 2017, in July.

The global radiation remained between 14.98 and 26.99 MJ m^{-2}, with the lowest and highest values observed in August 2010 and November 2015, respectively. The lowest global radiation values occurred between May and July (autumn and winter).

The relative air humidity ranged from 46% to 73%, presenting the lowest values in November 2015 and January 2017 and the highest in April 2008 and 2009.

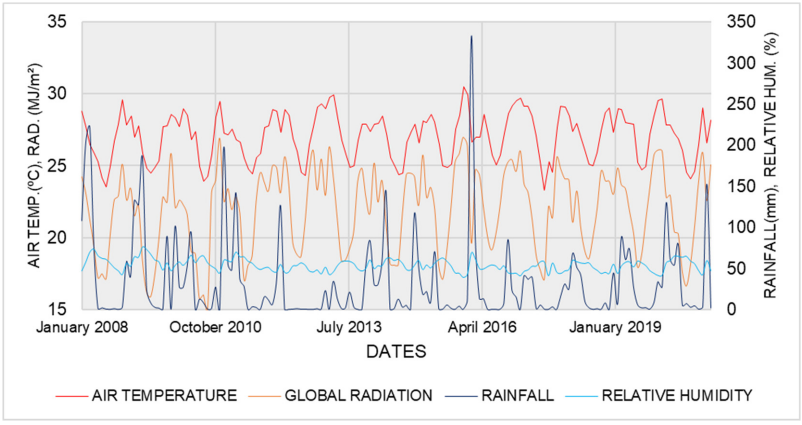

Figure 5. Meteorological data from the Meteorology Laboratory (LabMet) automatic weather station for the period 2008 to 2012, Juazeiro, Bahia, Brazil.

3.2. Classification of Land Use and Land Cover

Figure 6 shows the land use and land cover in the study area between 2006 and 2012. Sugarcane fields were the predominant vegetation, followed by savanna formation (Caatinga), water bodies, and forest formation. Between 2006 and 2011, sugarcane fields decreased and then expanded over areas of savanna formation. In 2012, sugarcane plantations expanded again, advancing over the savanna formation, occupying 100% of the study area. Water bodies (reservoirs) and irrigation canals were frequent in the watershed between 2006 and 2012. The savannah formation grew along with the water flow of the irrigation canals.

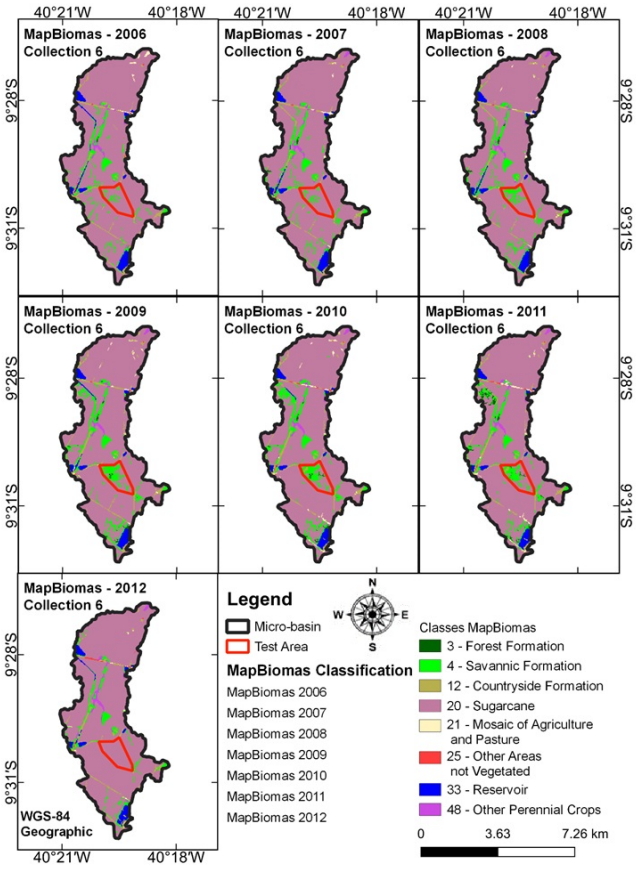

Figure 6. Classification of the land use and land cover of the watershed using MapBiomas in its Collection 6 (2006–2012).

Figure 7 shows the variations in the area (ha) cultivated with sugarcane between 2001 and 2020, in which the watershed presented two distinct moments. During the first moment, between 2001 and 2011, the area planted with sugarcane reached a maximum value of 2523.18 ha in 2003, reducing the area to 2360.05 ha in 2009. The second moment started in 2012, reaching a peak in the sugarcane cultivated area of 2566.85 ha in 2017 due to the implementation of change with new sugarcane varieties associated with interesting agro-industrial characteristics. After the first harvest (1998/1999, Table 1), the sugarcane was harvested annually for 14 years.

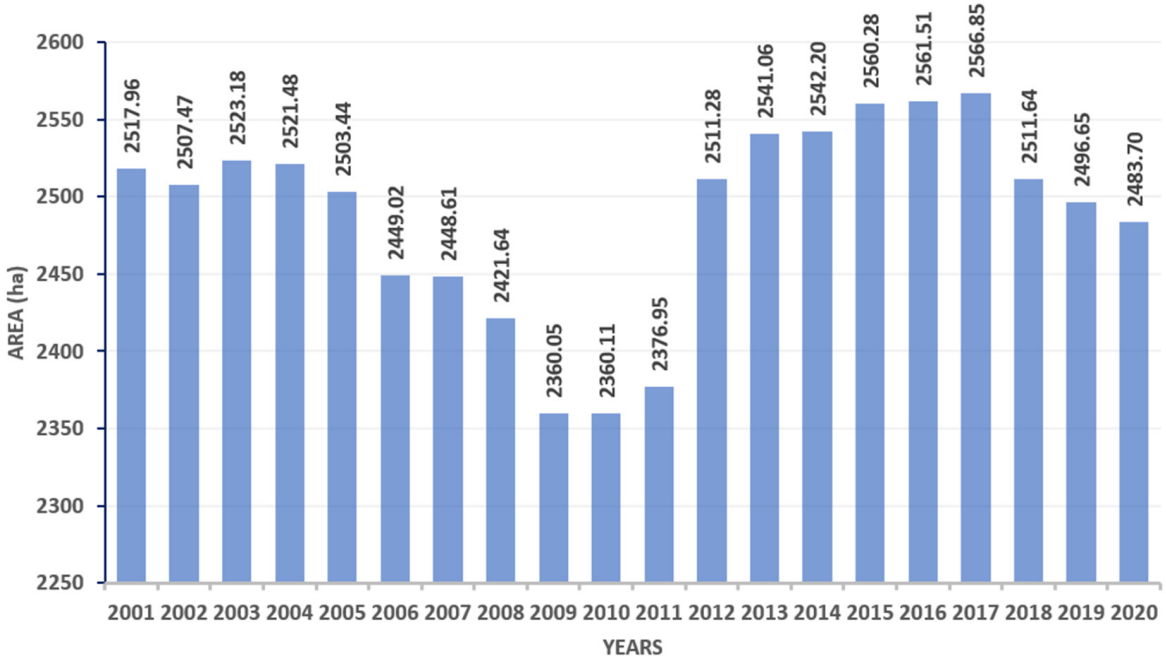

Figure 7. Temporal distribution of the area cultivated with sugarcane in the watershed from 2001 to 2020 in Juazeiro, Bahia, Brazil.

3.3. Normalized Difference Vegetation Index (NDVI) and Rainfall Time Series

Figure 8 shows the time series of rainfall (blue curve) and NDVI (green curve) in the study area. The variability of rainfall did not follow the behavior of NDVI. The sugarcane areas presented 19 phenological cycles between 2001 and 2020. The NDVI time series presents two distinct periods. The first period corresponds to 2001 to 2012, when the area was cultivated with the SP 79-1011 variety, indicating good productivity between the 12 phenological cycles, with higher NDVI amplitudes between 2002 and 2005. From 2006 onwards, the NDVI curve decreased, influencing the lower values of NDVI amplitudes between 2006 and 2012. The second period, containing seven phenological cycles between 2013 and 2020, was marked by an increase in the NDVI amplitude due to the renewal of the area with a replacement of the SP 79-1011 variety by the VAT 90-212 variety, justifying greater vegetative vigor of the sugarcane in its first year of cultivation.

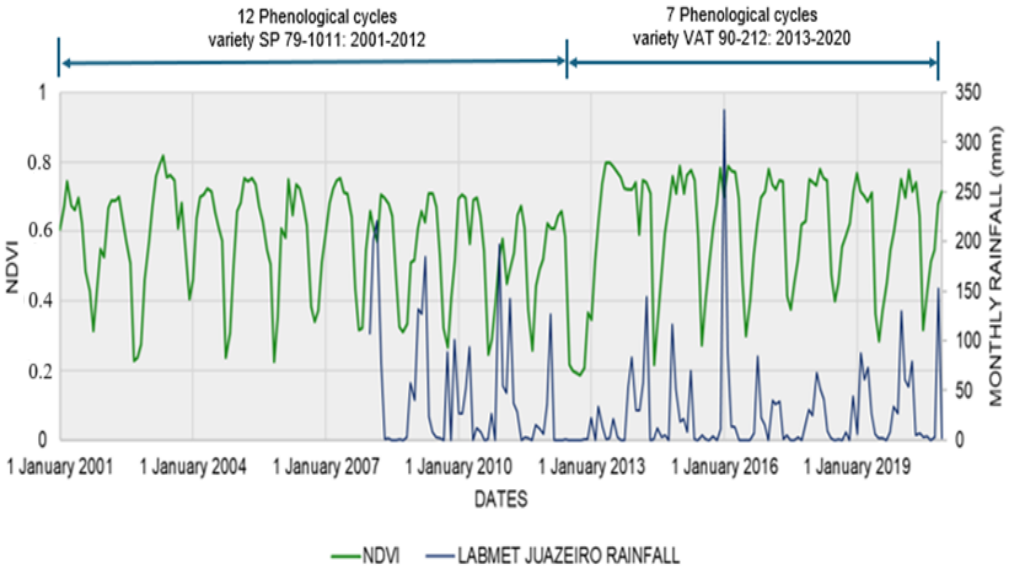

Figure 8. MODIS NDVI (2001–2020) for the total area and rainfall of Labmet Juazeiro (2008–2020) time series.

3.4. Sugarcane Phenological Parameters Estimated with the TIMESAT Software

Figure 9 shows the NDVI time series of sugarcane without and with the adjustment using the Savitsky–Golay filter of the TIMESAT software. The Savitsky–Golay filter omitted the bad NDVI pixels. In addition, the Savitsky–Golay filter indicated the start (blue dot) and the end (yellow dot) of the sugarcane phenological cycle.

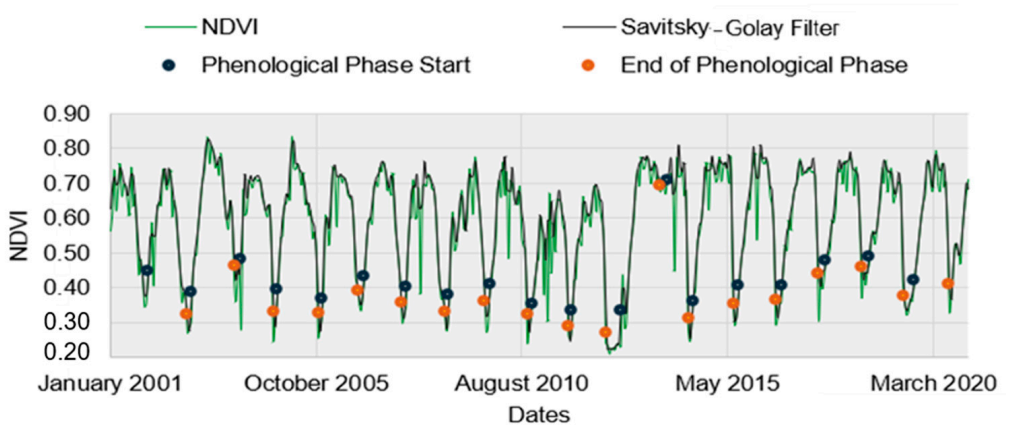

Figure 9. NDVI time series and Savitsky–Golay filter for the sugarcane total area. The dots represent the start (in blue) and the end (in yellow) of the sugarcane phenological cycles.

Table 4 illustrates the phenological parameters of the sugarcane area estimated by the TIMESAT software, using the NDVI time series between 2001 and 2020. Column 1 represents the 19 phenological cycles (Season) of the sugarcane, columns 2 and 3 the dates of the start (a) and end (b) of the crop years, respectively. The most frequent month for the start of the crop growing season with the variety SP 79-1011 was November, while the variety VAT 90-212 presented the month of August. The end of the phenological cycle for variety SP 79-1011 was between September and October, while variety VAT90-212 varied between June and July.

Table 4. Phenological parameters obtained with TIMESAT software for the study area.

Seasons	SOS	EOS	LOS (Days)	e	POS	f	I	F
1	17 November 2001	13 October 2002	332	25 April 2002	0.74	0.41	0.45	0.32
2	21 November 2002	21 November 2003	368	16 May 2003	0.82	0.47	0.38	0.46
3	11 January 2004	21 October 2004	285	27 May 2004	0.72	0.36	0.48	0.33
4	19 November 2004	05 November 2005	354	28 April 2005	0.81	0.53	0.39	0.32
5	04 Dezember 2005	03 October 2006	305	04 May 2006	0.75	0.43	0.37	0.39
6	24 November 2006	11 October 2007	322	12 May 2007	0.75	0.42	0.43	0.35
7	17 November 2007	14 October 2008	334	09 April 2008	0.75	0.46	0.40	0.33
8	16 November 2008	20 September 2009	309	08 June 2009	0.76	0.46	0.37	0.36
9	04 November 2009	19 September 2010	322	07 April 2010	0.77	0.47	0.40	0.32
10	26 October 2010	05 September 2011	317	10 April 2011	0.67	0.41	0.35	0.29
11	01 October 2011	20 July 2012	296	20 Match 2012	0.69	0.46	0.33	0.27
12	17 November 2012	19 October 2013	339	15 May 2013	0.77	0.32	0.33	0.69
13	14 Dezember 2013	19 June 2014	189	17 April 2014	0.80	0.33	0.71	0.31
14	26 July 2014	07 July 2015	349	14 February 2015	0.77	0.49	0.36	0.35
15	19 August 2015	02 July 2016	319	15 February 2016	0.80	0.49	0.40	0.36
16	17 August 2016	26 June 2017	316	27 February 2017	0.76	0.40	0.40	0.44
17	25 August 2017	02 July 2018	314	24 February 2018	0.78	0.37	0.48	0.45
18	30 August 2018	25 June 2019	301	01 Match 2019	0.76	0.38	0.49	0.37
19	19 September 2019	13 July 2020	301	13 Match 2020	0.78	0.43	0.42	0.40
Minimum			189		0.67	0.33	0.33	0.27
Maximum			368		0.82	0.53	0.71	0.46
Mean			313		0.76	0.43	0.42	0.36

where: SOS = Date of the Start Of the Station; EOS = Date of the End Of the Station; e = Date with the highest adjusted NDVI value; POS = Peak Of Season (NDVI Peak); f = Seasonal NDVI amplitude; LOS = Length of the Season (days); I = The NDVI at the start of the Seasonal; F = the NDVI at the end of the Seasonal. And the 2003/2002 crop had a long phenological cycle, lasting 368 days (Table 4). However, the 2013/2014 crop had the shortest growing and development season, making up 182 days. The average duration of the phenological cycles was 312 days.

The information in Table 4 enabled the construction of an agricultural calendar for the varieties SP 79-1011 and VAP 90-212 illustrated in Figure 10. For the variety of sugarcane (SP 79-1011) planted between 2001 and 2012, the emergence phase occurred in October, the establishment phase occurred from October to November with the maximum development phase from April to June, and the harvest was scheduled between September and October. The new variety VAP 90-212 emerged in July and established itself in August, maximum development occurred between February and March, and harvest is expected from June to July from 2012 to 2020.

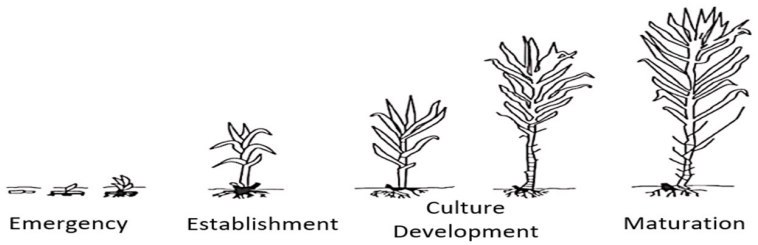

Variety SP 79–1011 (2001–2012)										
Activities	**Feb**	**Mar**	**Apr**	**May**	**Jun**	**Jul**	**Aug**	**Sep**	**Oct**	**Nov**
Emergency									■	
Establishment									■	■
Max. Development			■	■	■					
Harvest								■	■	
Variety VAP 90–212 (2012–2020)										
Activities	**Feb**	**Mar**	**Apr**	**May**	**Jun**	**Jul**	**Aug**	**Sep**	**Oct**	**Nov**
Emergency						■				
Establishment							■			
Max. Development	■	■								
Harvest					■	■				

Figure 10. Sugarcane agricultural calendar in the test area from the SP 79-1011 and VAP 90-212. In blue, months referring to the phenological phases of sugarcane.

3.5. Statistical tests

The Shapiro–Wilks test verifies whether the harvest dates of the 13 plots and the total sugarcane area followed a normal distribution. The harvest dates of all sugarcane cultivated plots, except plot 7, follow a normal distribution since the *p*-value values of the Shapiro–Wilks test were less than 0.05, i.e., for a significance level of 5%. The Accept H0 hypothesis evidences that the sugarcane harvest dates of all areas, except for sugarcane field 7, follow a normal distribution.

An analysis of the parametric test (Student's *t*-test), including sugarcane field 7, resulted in all sugarcane areas accepting the null hypothesis. This is, for the harvest dates observed and those estimated with the TIMESAT software, there was no difference between the average dates of the compared groups, at a significance level of 5% (*p*-value > 0.05).

3.6. Validation of Estimated Harvest Dates with TIMESAT Software

Figure 11 shows the validation of the harvest dates observed and estimated by the TIMESAT software. The convention of dates (day, month, and year) in days of the year made it possible to plot the observed and estimated harvest dates. The points were close to the linear regression line (1:1), indicating an excellent fit between the observed and estimated harvest dates.

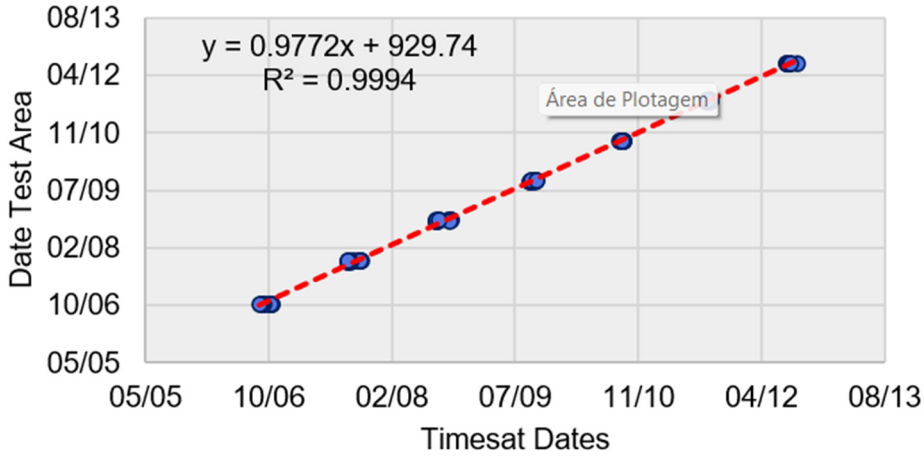

Figure 11. Comparison of variety SP 79-1011 harvest dates observed with estimated values with TIMESAT software for the test area between 2006 to 2012.

Table 5 illustrates the statistical parameters for the observed and estimated harvest dates of the 13 areas and the total sugarcane area. The study area presented a Pearson correlation (*r*) equal to 0.99 (almost perfect), coefficient of determination (r^2) of 0.99, agreement index (d) of 0.99, index of performance (e) equal to 0.99 (classified as excellent), tendency to underestimate values (ME) equal to –3.92 days), mean absolute error (MAE) of 10.45 days with root mean square error (RMSE) of 11.87 days.

The 13 sugarcane areas presented a correlation coefficient close to 1 (Table 5). Therefore, these plots were classified as having a near-perfect correlation, indicating that the TIMESAT software accurately estimated the sugarcane harvest dates. Sugarcane fields 1, 3, 4, and 7 showed a lower MAE or a higher precision ranging between 4 and 9 days. Regarding the performance index (e), the best results occurred in sugarcane plots 1, 3, 4, and 7, while for the other plots, the values of e were equal to 0.99, classified as Excellent, indicating that the determination of dates with the TIMESAT software accurately estimated this variable.

Table 5. Statistical parameters of the 13 plots that make up the test area.

PAI	Hectares	*r*	R^2	ME	MAE (Days)	RMSE (Days)	Performance *r*	d	e	Performance e
1	11.64	0.99	0.99	−7.51	7	10	Almost Perfect	0.99	0.99	Great
2	8.07	0.99	0.99	−11.62	12	13	Almost Perfect	0.99	0.99	Great
3	9.89	0.99	0.99	−3.45	5	8	Almost perfect	0.99	0.99	Great
4	10.27	0.99	0.99	−2.06	4	5	Almost perfect	0.99	0.99	Great
5	11.19	0.99	0.99	−12.52	26	32	Almost perfect	099	0.99	Great
6	10.16	0.99	0.99	−23.56	26	33	Almost perfect	0.99	0.99	Great
7	11.10	0.99	0.99	−8.38	8	9	Almost perfect	0.99	0.99	Great
8	9.71	0.99	0.99	−22.07	25	35	Almost perfect	0.99	0.99	Great
9	9.26	0.99	0.99	−26.01	27	37	Almost perfect	0.99	0.99	Great
10	6.88	0.99	0.99	−23.43	26	34	Almost perfect	0.99	0.99	Great
11	7.51	0.99	0.99	−25.30	27	37	Almost perfect	0.99	0.99	Great
12	7.85	0.99	0.99	−28.53	29	40	Almost perfect	0.99	0.99	Great
13	7.97	0.99	0.99	−24.90	28	39	Almost perfect	0.99	0.99	Great
Total area	121.5	0.99	0.99	−3.92	10	11	Almost perfect	0.99	0.99	Great

where: PAI: plot area identifier; *r*: Pearson correlation coefficient, R^2: adjusted coefficient of determination, ME: mean error, MAE: mean absolute error, RMSE: root mean square error, d: Willmott's (1985) [74] concordance index, e: Camargo and Sentelhas [75] performance index, and Performance r: Pearson's correlation coefficient rank (*r*).

4. Discussion

4.1. Use of the MOD13Q1 Product

The choice between the MODIS sensor (MOD13Q1 product), Landsat 5, 7, 8, and 9, Sentinel 1, and Sentinel 2 depends on several factors, including the research objectives, the scale of the analysis, and the specific characteristics of the images. However, Justice et al. [45] cite the following as imperative characteristics of the MODIS sensor: revisit time, global coverage, large-scale applications, productivity and cost, product diversity, cloud resistance, and spectral resolution.

The MODIS sensor is onboard the Terra and Aqua satellites, which makes it possible to obtain two daily scenes of the same area, increasing the possibility of capturing images with minimal cloud cover. However, temporal resolutions of the Landsat 5, 7, 8, and 9 are 16 days, Sentinel-1 is 12 days, while Sentinel-2 is five days [29,46,76], increasing the chances of capturing images with clouds in the study area. The moderate spatial resolution of the MODIS sensor is capable of capturing vegetation trends and patterns without the need for higher resolutions [45,77]. Furthermore, the images from the MODIS sensor and its MOD13Q1 product enable the construction of time series for continuous observations of dynamic phenomena [45,78], such as seasonal changes in sugarcane phenology [11,28].

MODIS sensor images are often made available free of charge and automatically generated, facilitating access and use in large volumes [18]. Therefore, the MODIS sensor has these advantages in terms of cost and efficiency compared to higher-resolution data that may require more processing and storage [47]. The MODIS sensor offers many products, including vegetation indices, surface temperature, albedo, and others, useful in environmental analyses [10].

The MOD13Q1 product contains the Normalized Difference Vegetation Index (NDVI) and Enhanced Vegetation Index (EVI) vegetation indices. They are produced globally with 1 km, 500 m, and 250 m resolutions in a composition of 16-day Terra satellite images or mosaics, increasing the possibility of obtaining cloud-free images. These indexes allow studies to be carried out on vegetation cover on a spatial-temporal scale, describing and reconstructing data on phenological variations and discriminating interannual variations in vegetation on global and regional scales [78].

The NDVI is more sensitive to the presence of chlorophyll and other plant pigments, which are responsible for absorbing solar radiation in the red band [41]. It is the most widely used index in various studies on vegetation that involve the use of remote sensing data [79]. The NDVI is a ratio of the difference in reflectance measurement (ρ) in the near-

infrared (0.70–1.30 µm) and red (0.55–0.70 µm) channels and the sum of these channels [80], that is: NDVI = (ρNIR − ρR)/(ρIVP + ρR), where ρIVP corresponds to the spectral response of the pixel in the near-infrared band, and ρR corresponds to the spectral response of the pixel in the visible red band. The NDVI value can vary on a scale between +1 to −1, and the closer to +1, the greater the density of vegetation cover.

Although the Landsat 5, 7, 8, and 9 satellites have spatial resolutions of 15 and 30 m, as well as Sentinel 1 with 10 m and Sentinel 2 with 20 m, the choice of the MOD13Q1 product is more suitable for the present study, as it prioritizes a high revisit time.

4.2. MOD13Q1 Product Pixel Treatments

Images from orbital sensors can result from several external influences, including (1) instrument calibration and characteristics; (2) clouds and cloud shadows; (3) atmospheric effects due to variable aerosols, water vapor, and residual clouds; (4) sensor–target–sun geometric configurations and (5) interactions resulting from surface anisotropies, and (6) atmospheric-dependent angular response, among others [78]. Given these influences, the definitions of the MODIS sensor characteristics, the data generated, and the distribution of its products were carefully designed and planned through the international program called Earth Observing System (EOS), led by the National Aeronautics and Space Administration (NASA) for global change studies [81].

The MODIS sensor data are made available in the shape of products to facilitate their use in several application areas. The images of the sensor spectral bands are geometrically, atmospherically, and radiometrically corrected. In addition, they are transformed into vegetation indices, among others [82]. To ensure the quality of MODIS products, they go through several versions called collections. The current version is collection 6.1, which has changes in the programs that generate the products (https://lpdaac.usgs.gov/data/, accessed on 27 June 2022). Whenever a new version is made available, the data are processed again to maintain compatibility between previous and current data [82].

The MOD13Q1 product uses the MOD09 product as input data. This product is an estimate of surface reflectance, computing from level 1A in bands 1, 2, 3, 4, 5, 6, and 7 with wavelengths centered at 0.648 µm, 0.858 µm, 0.470 µm, 0.555 µm, 1.240 µm, 1.640 µm, and 2.130 µm, respectively. These bands are defined for a study of the Earth's surface [45]. To ensure the integrity of the MOD13Q1 product, the quality control with information about each pixel accompanies the reflectance estimates (Table 6).

Table 6. Quality assessment (QA) for each pixel of MOD13Q1 product.

QA	Performance
0	Good quality
1	Undefined quality
2	Produced, but most probably cloudy
3	Not produced due to other reasons than clouds
6, 7	Produced due to aerosol quantity
9	Atmospheric correction
10	Not produced due to cloud effects
11, 12, 13	Not produced due to shadow effects
15	Not produced due to shadow effects

Source: adapted from https://lpdaac.usgs.gov/data, accessed on 30 January 2022.

4.3. Meteorological Variables and Sugarcane

The main meteorological variables that influence the growth, development, and productivity of sugarcane include rainfall, air temperature, solar radiation, air humidity, among others [83–85].

In the study area, rainfall is irregular and poorly distributed [58], which can harm the cultivation and harvesting of sugarcane. The best time to grow sugarcane in the region is between February and March, avoiding the rainy season [86]. Rain acts indirectly, affecting

both the growth and development of crops, in addition to the water availability of the soil, which in turn, influences the absorption of water by the roots and the water status of the crops [83]. Rainfall negatively affects the sugar content in sugarcane stalks and creates difficulties with manual harvesting [87]. However, periods of excessive rainfall compromise soil oxygenation, resulting in decreased root activity and reduced absorption of water and nutrients by plants. In periods of little rainfall, drought causes plants to close their stomata, fixing less CO_2 and negatively affecting photosynthesis [88]. Sugarcane can be harvested during the dry period from April to January [89] when the harvested material's moisture content is low and the sucrose concentration is higher [90]. In addition, rainfall during the sugarcane harvest season seriously hinders the planning of cutting, harvesting, and transportation from the field to the industry.

Air temperature also affects several other processes in plants, such as maintenance respiration, transpiration, vegetative rest, the duration of crop phenological phases, flowering induction, oil content in grains, seed germination rate, etc. [84,85]. In the study area, the average air temperature varies between 25 °C and 30 °C throughout the year [57]. This thermal condition is appropriate for sugarcane cultivation since the air temperature range of 23 °C to 32 °C is ideal for increasing photosynthetic activity and sugarcane growth [91]. The species' respiration is at maximum between 36 °C and 38 °C, which means that above 33 °C, dry matter gain tends to decrease to a point where it becomes practically zero, with temperatures close to 38 °C [92]. The optimum temperature for tillering is between 27 °C and 32 °C, and at temperatures below 5 °C and above 45 °C, the process is practically paralyzed [93]. During the maturation phase, lower temperatures concentrate sucrose in the stalk, which can replace water deficiency as a determining factor at the beginning of the process [92].

The availability of incident solar radiation in the study area is high. Marin et al. [92] explain that sugarcane is a species with a C4 photosynthetic cycle, presenting high efficiency in the conversion of radiant energy into chemical energy when subjected to conditions of high air temperature and intense solar radiation, associated with high availability of water in the soil. Fauconnier et al. [91] state that sugarcane fields cultivated in regions with intense solar radiation have a larger leaf area, thicker and greener leaves, and more developed roots, tending to accumulate more dry matter (sugar and fiber) to the detriment of the amount of water. During germination, there is no evidence that solar radiation affects the development of sugarcane buds, which can germinate even without radiation [91]. However, in the vegetative development phase, several events are influenced by radiation. Tillering, for example, is favored by intense solar radiation [94].

Sugarcane is an essentially tropical plant grown in regions where relative humidity varies from 40% to 80% [95]. On average, the sugarcane fields in this study are within this optimal relative humidity range. However, the study area is susceptible to days with low relative humidity. In dry environments, this leads to an excessive increase in transpiration in most plants, which can cause indirect damage resulting from physiological disorders [86]. In addition to these aspects, Sentelhas [90] highlights that air humidity plays a crucial role in the interaction between plants and microorganisms, especially fungi and bacteria, causing various diseases. In conditions of high humidity, where the duration of leaf wetness is longer, there is a greater risk of diseases that affect crop performance, reducing the quantity and quality of agricultural products.

4.4. Analysis of Classification of Land Use and Land Cover

The annual classification of the land use and land cover for the study area showed sugarcane as the predominant vegetation cover, followed by savanna formation (Caatinga), water bodies, and forest formation. In the study area, sugarcane fields expanded over the years, advancing over the savanna formation. According to Santos et al. [94], in Juazeiro, Bahia, even in the semi-arid climate, sugarcane has been produced in large territorial extensions, irrigated with water collected from the São Francisco River and tributaries. Soares et al. [96] highlight that the increase in sugarcane plantations may be associated

with the edaphoclimatic conditions of the Brazilian semi-arid region combined with water availability and irrigation technologies. However, replacing a preserved Caatinga area with irrigated sugarcane cultivation increases the surface albedo, reducing radiation absorption and energy availability at the surface [97]. Souza et al. [98] also observed that the conversion of Caatinga into pasture acquires biophysical characteristics that imply a reduction in the radiation balance compared to Caatinga with forest formation. This reduction is substantially due to an increase in the average albedo value, which remains higher, even in the rainy seasons [98]. The water bodies (reservoirs) supply the irrigation systems by the center pivot, furrow, or drip throughout the watershed [96]. In the study area, the drip irrigation system supplies the plant with greater sustainability [96].

4.5. Analysis of Normalized Difference Vegetation Index (NDVI) and Rainfall Time Series

The NDVI time series did not follow the rainfall time series in the study area. In the study area, the sugarcane fields were irrigated with water from the São Francisco River and did not depend on the scarce regional rainfall regime, which reaches 600 mm per year [58]. Sugarcane plantations consume more than 1500 mm of water per crop cycle, requiring supplemental irrigation [22]. Gunnula et al. [99] also found similar results, observing that the temporal changes in the NDVI of 2854 irrigated sugarcane fields did not follow the rainfall regime in northeastern Thailand.

In addition, rainfall in the study area is irregular and poorly distributed annually [58]. Continuous monitoring of rainfall is necessary to avoid a direct impact on operational planning for the harvest, compromising the cutting and transportation of sugarcane. Marin et al. [92] mention the interruption or slowdown of fieldwork on rainy days and the increase in soil moisture during periods when machinery traffic is heavy, which can cause intense soil compaction, potentially reducing sugarcane productivity. Aguiar et al. [100] add that the main impediment to the regular progress of sugarcane cutting in the cultivated area throughout the harvest period is the occurrence of rain, especially long-lasting rain, as it directly affects the traffic of machines involved in both crop cutting, whether for a mechanized harvester or in transporting the sugarcane from the field to the industry.

Regarding systems that use fire as a sugarcane management strategy, Marin et al. [92] mention that rainfall affects soil quality during harvesting, as it is more pronounced than those observed in harvesting systems without burning, which are usually mechanical. Ceddia et al. [101] explain that fire favors soil exposure to rain and vehicle traffic, with a reduction in the average diameter of aggregates, an increase in density in the most superficial layers, and a decrease in the speed of water infiltration.

4.6. Analysis of Sugarcane Phenological Parameters Estimated with the TIMESAT Software

The analysis of sugarcane phenological parameters will help rural producers organize their prevention activities, reducing the risk of crop losses due to unexpected rainfall events. Rainfall in sugarcane fields in the study area can occur between November and February, but is insufficient to reduce the regional water deficit [102]; even so, there is no reduction in sugarcane productivity, as the monoculture receives supplementary irrigation [30]. According to Silva et al. [4], the SP 79-1011 variety is sensitive to soil water variability, directly impacting physiological functions and reducing productivity due to photosynthetic reduction. However, VAT 90-212 variability is common in areas with high soil moisture [103], showing good adaptation in soils with low moisture and a positive physiological response without significantly affecting its productivity.

The agricultural calendar's function guides rural producers regarding the best dates for planting and harvesting sugarcane. In this study, planting dates were between October to July, and harvest dates were between September to October or June to July, depending on the variety. In Brazil, sugarcane is regularly planted between September and October and harvested between November and May of the following year, depending on the maturity time of the variety used. It spends an average of 18 months in the field [93]. According to CONAB [103], in Bahia, Brazil, sugarcane from the 2018/2019 and 2019/2020 harvests was

harvested between April and June, corroborating the harvest date of VAT 90-212. In São Paulo, Brazil, sugarcane is harvested 18 months after summer planting and 12 months after winter planting [104]. At harvest, stalks that remain in the soil sprout, and new plants grow and develop, repeating the phenological cycle [29]. In each successive phenological cycle, the yield of sugarcane fields decreases. Baghdadi et al. [104] cite a limit of five to seven consecutive harvests for replanting a sugarcane variety.

4.7. Statistical Evaluation

The Shapiro–Wilk test is essential to assess whether sugarcane harvest dates follow a normal distribution. In addition, a Student's *t*-test determines whether there is a significant difference between the means of the sugarcane dates. In general, sugarcane harvest dates followed a normal distribution, and the acceptance of the null hypothesis (equal means) was true for the study area. Lisboa et al. [105] applied the Shapiro–Wilks test to verify whether changes induced by straw removal rates (0, 25, 50, and 100%) affect sugarcane productivity in São Paulo, Brazil. The authors reject the hypothesis of normal distribution when the *t*-test is significant. They showed that straw removal rates do not linearly affect sugarcane productivity but depend on site-specific characteristics related to soil, climate, and variety.

4.8. Analysis of Estimated Harvest Dates with TIMESAT Software

The validation of sugarcane harvest dates included mean error, mean absolute error, and root mean square error, among others. The study area (121.5 ha) presented a mean absolute error of 10 days in estimating the sugarcane harvest date. Only four plots in the study area presented a mean absolute error of less than ten days. One reason for this discrepancy is the pixel size of the MOD13Q1 product, which was 250 m (6.25 ha) in spatial resolution. Oré et al. [106] predicted the harvest date of sugarcane (RB975952), which has a nominal cycle of 18 months, using a system based on Synthetic Aperture Radar (SAR) installed on the drone in four areas of the municipality of Iracemápolis, São Paulo, Brazil. The authors [106] used a biomass image histogram to estimate the sugarcane harvest dates, resulting in a mean error of 8 days. Stasolla et al. [29] presented a method for automatic estimation (Continuous Wavelet Transform) of sugarcane harvest dates using a time series of Sentinel-1 SAR GRD (C-band Synthetic Aperture Radar Ground Range Detected) products. The technique applied to 719 sugarcane plots in Northern Senegal produced an average mean absolute error in estimating the sugarcane harvest date of less than five days, achieving greater accuracy than the Sentinel-1 revisit frequency for the region considered (12 days) [29].

5. Conclusions

The phenological metrics represent the characteristics of the vegetation within its phenological cycle, corresponding to dimensionless output parameters and can be calculated based on the NDVI time series. In this study, the TIMESAT software was used to analyze 19 years of NDVI time series and to compute phenological metrics: Start of Season (SOS), End Of Season (EOS), Length of the Season (LOS), and Peak of Season (POS), among others. The TIMESAT software was able to estimate phenological parameters in areas cultivated with sugarcane in the São Francisco Valley, Bahia, Brazil, using Google Earth Engine to process images of MOD13Q1 NDVI between the years 2001 to 2020, satisfactorily.

The annual classification of land use and land cover of the study area showed that sugarcane is the predominant vegetation cover, followed by savanna formation (Caatinga), water bodies, and forest formation. The expansion of sugarcane plantations has advanced over the savanna formation. The savanna formation existing in the area follows the irrigation channels. Fragments of forest formation are still present in the area. The water bodies serve to store water used to irrigate the sugarcane fields.

The MOD13Q1 NDVI time series of sugarcane fields did not accompany the rainfall observed in the study area. In irrigated sugarcane fields in the semi-arid region, the rainfall

regime is irregular and poorly distributed, and these rains are undesirable during harvesting, negatively influencing harvest dates and directly harming production. Continuous monitoring will avoid rain on sugarcane harvest dates.

The Savitsky–Golay filter best adjusted the MODIS NDVI time series, minimizing atmospheric interference in the data. This filter indicated the beginning and end of 19 phenological cycles, 12 cycles referring to the SP 79-1011 variety, and seven cycles to VAT 90-212 between 2001 and 2020. According to the Shapiro–Wilk and Student *t*-tests, sugarcane harvest dates follow a normal distribution, and the acceptance of the null hypothesis (equal means) was true for the study area. Furthermore, the study area presented a Pearson correlation of 0.99 (almost perfect), a coefficient of determination of 0.99, a Willmott concordance index of 0.99, a performance index of 0.99 (classified as excellent), a tendency to underestimate values (ME of -3.92 days), and a root mean square error (RMSE) of 11.87 days.

The mean absolute error obtained to predict the sugarcane harvest date in the study area was approximately ten days greater than those estimated by Sentinel-1 and SAR on board high spatial resolution drones. However, the TIMESAT software performed well in estimating the sugarcane harvest date with the MOD13Q1 NDVI product. The MOD13Q1 NDVI product integrated with the TIMESAT software can be used by producers in operational mode in sugarcane production processes with caution if the area is superior to 6.25 ha, pixel size (250 m) of the MOD13Q1 NDVI.

Author Contributions: D.R.C.M.: Conceptualization, Investigation, Writing—Review and Editing, Visualization, Supervision; P.M.O.L.: Conceptualization, Methodology, Validation, Formal analysis, Investigation, Data Curation, Writing—Original Draft, Writing—Review and Editing, Visualization, Supervision; C.R.N.: Writing—Review and Editing, Visualization; E.P.R.: Writing—Review and Editing, Visualization; A.S.d.S.: Writing—Review and Editing, Visualization, Supervision. All authors have read and agreed to the published version of the manuscript.

Funding: We thank the Postgraduate Program in Agricultural Engineering at the Federal Rural University of Pernambuco (UFRPE) for the logistics necessary for this research. We also thank the Coordination for the Improvement of Higher Education Personnel, Brazil (CAPES) for granting a scholarship, funding code 001.

Data Availability Statement: The datasets generated during and/or analyzed during the current study are available from the corresponding author upon reasonable request.

Acknowledgments: We thank AGROVALE, NASA's Land Processes Distributed Active Archive Center (LP DAAC) for granting data, the Google Earth Engine computational platform.

Conflicts of Interest: The authors declare no competing interests.

References

1. Oliveira, D.M.; Cherubin, M.R.; Franco, A.L.; Santos, A.S.; Gelain, J.G.; Dias, N.M.; Diniz, T.R.; Almeida, A.N.; Feigl, B.J.; Davies, C.A.; et al. Is the expansion of sugarcane over pasturelands a sustainable strategy for Brazil's bioenergy industry? *Renew. Sustain. Energy Rev.* **2019**, *102*, 346–355. [CrossRef]
2. Shi, C.; Xie, C.; Zhang, Z.; Rackemann, D.; Wei, B.; Hang, F.; Lu, H.; Li, K.; Doherty, W.O. Sugar and value-added products derived from retentate concentrate of sugarcane juice. *J. Clean. Prod.* **2020**, *278*, 123915. [CrossRef]
3. Almeida, L.J.M.; Silva, A.V.; Silva, J.S.L.; Silva, J.F.; Silva, J.H.B.; Pereira Neto, F.; Borba, M.A.; Barreto, S.S.C.; Rodrigues, H.A.; Sousa, V.F.O.; et al. Sugarcane productivity and economic viability in response to planting density. *Braz. J. Biol.* **2024**, *84*, 1–7. [CrossRef]
4. Silva, D.F.d.S.; Bomtempo, J.V.; Alves, F.C. Innovation opportunities in the Brazilian sugar-energy sector. *J. Clean. Prod.* **2019**, *218*, 871–879. [CrossRef]
5. União Nacional da Bioenergia—UDOP. Cogeração de Energia a Partir de Biomassa Cresce 8% no Primeiro Trimestre de 2024. Available online: https://www.udop.com.br/noticia/2024/05/24/cogeracao-de-energia-a-partir-de-biomassa-cresce-8-no-primeiro-trimestre-de-2024.html (accessed on 29 June 2024).
6. CONAB (Companhia Nacional de Abastecimento). *Monitoring the Brazilian Sugarcane Harvest*; CONAB: Brasília, Brazil, 2024. Available online: www.conab.gov.br (accessed on 29 June 2024).
7. AGROVALE (AgroIndústrias do Vale do São Francisco, S.A). AGROVALE: Juazeiro, Bahia, Brazil. 2024. Available online: https://agrovale.com/ (accessed on 1 August 2024).

8. Heupel, K.; Spengler, D.; Itzerott, S.A. Progressive Crop-Type Classification Using Multitemporal Remote Sensing Data and Phenological Information. *PFG–J. Photogramm. Remote Sens. Geoinf. Sci.* **2018**, *86*, 53–69. [CrossRef]
9. Mas, J.-F.; Soares de Araújo, F. Assessing Landsat Images Availability and Its Effects on Phenological Metrics. *Forests* **2021**, *12*, 574. [CrossRef]
10. Rudorff, B.F.T.; Aguiar, D.A.; Silva, W.F.; Sugawara, L.M.; Adami, M.; Moreira, M.A. Studies on the Rapid Expansion of Sugarcane for Ethanol Production in São Paulo State (Brazil) Using Landsat Data. *Remote Sens.* **2010**, *2*, 1057–1076. [CrossRef]
11. Kumar, S.; Meena, R.S.; Sheoran, S.; Jangir, C.K.; Jhariya, M.K.; Banerjee, A.; Raj, A. Chapter 5—Remote sensing for agriculture and resource management. In *Natural Resources Conservation and Advances for Sustainability*; Elsevier: San Diego, CA, USA, 2022; pp. 91–135.
12. Campbell, J.B.; Wynne, R.H. *Introduction to Remote Sensing*, 5th ed.; Guilford Press: New York, NY, USA, 2011.
13. De Beurs, K.; Henebry, G. Land surface phenology, climatic variation, and institutional change: Analyzing agricultural land cover change in Kazakhstan. *Remote Sens. Environ.* **2004**, *89*, 497–509. [CrossRef]
14. Morisette, J.T.; Richardson, A.D.; Knapp, A.L.; Fisher, J.I.; Graham, E.A.; Abatzoglou, J.; Wilson, B.E.; Breshears, D.D.; Henebry, G.M.; Hanes, J.M.; et al. Tracking the rhythm of the seasons in the face of global change: Phenological research in the 21st century. *Front. Ecol. Environ.* **2008**, *7*, 253–260. [CrossRef]
15. Berra, E.F.; Gaulton, R. Remote sensing of temperate and boreal forest phenology: A review of progress, challenges and opportunities in the intercomparison of in-situ and satellite phenological metrics. *For. Ecol. Manag.* **2021**, *480*, 118663. [CrossRef]
16. Jayawardhana, W.G.N.N.; Chathurange, M. Extraction of Agricultural Phenological Parameters of Sri Lanka Using MODIS, NDVI Time Series Data. *Procedia Food Sci.* **2016**, *6*, 235–241. [CrossRef]
17. Zeng, L.; Wardlow, B.D.; Xiang, D.; Hu, S.; Li, D. A review of vegetation phenological metrics extraction using time-series, multispectral satellite data. *Remote Sens. Environ.* **2020**, *237*, 111511. [CrossRef]
18. Weiss, M.; Jacob, F.; Duveiller, G. Remote sensing for agricultural applications: A meta-review. *Remote Sens. Environ.* **2020**, *236*, 111402. [CrossRef]
19. Jung, J.; Maeda, M.; Chang, A.; Bhandari, M.; Ashapure, A.; Landivar-Bowles, J. The potential of remote sensing and artificial intelligence as tools to improve the resilience of agriculture production systems. *Curr. Opin. Biotechnol.* **2021**, *70*, 15–22. [CrossRef]
20. Ji, Z.; Pan, Y.; Zhu, X.; Wang, J.; Li, Q. Prediction of crop yield using phenological information extracted from remote sensing vegetation index. *Sensors* **2021**, *21*, 1406. [CrossRef]
21. Xin, F.; Xiao, X.; Cabral, O.M.R.; White, P.M., Jr.; Guo, H.; Ma, J.; Li, B.; Zhao, B. Understanding the Land Surface Phenology and Gross Primary Production of Sugarcane Plantations by Eddy Flux Measurements, MODIS Images, and Data-Driven Models. *Remote Sens.* **2020**, *12*, 2186. [CrossRef]
22. Park, S.; Robertson, M.; Inman-Bamber, N.G. Decline in the growth of a sugarcane crop with age under high input conditions. *Field Crop. Res.* **2005**, *92*, 305–320. [CrossRef]
23. Instituto Brasileiro de Geografia e Estatística (IBGE). Herds and Value of Products of Animal Origin Hit Record in 2022. Available online: https://agenciadenoticias.ibge.gov.br/en/agencia-news/2184-news-agency/news/37941-rebanhos-e-valor-dos-principais-produto-de-origem-animal-foram-recordes-em-2023 (accessed on 26 September 2024).
24. Maschio, R.; Coelho, R.D.; Barros, T.H.d.S.; Costa, J.d.O.; Duarte, S.N. Water rights in sugarcane irrigation: Influence of irrigation criteria and probability levels adopted for ETo and rainfall. *Sci. Agric.* **2024**, *81*, e20230139. [CrossRef]
25. Saath, K.C.d.O.; Fachinello, A.L. Crescimento da demanda mundial de alimentos e restrições do fator terra no Brasil. *Rev. Econ. Sociol. Rural* **2018**, *56*, 195–212. [CrossRef]
26. Grunow, M.; Gnther, H.O.; Westinner, R. Supply optimization for the production of raw sugar. *Int. J. Prod. Econ.* **2007**, *110*, 224–239. [CrossRef]
27. Simões, W.L.; Calgaro, M.; Guimarães, M.J.M.; Mliveira, A.R.; Pinheiro, M.P.M.A. Sugarcane crops with controlled water deficit in the Submiddle São Francisco Valley, Brazil. *Rev. Caatinga* **2018**, *31*, 963–971. [CrossRef]
28. Silva, A.S.; Costa, M.A.; Moura, G.B.A.; Lopes, P.M.O.; Guimarães, M.J.M.; Gomes, A.W.A. Agrometeorological-spectral model for estimating sugarcane productivity in Brazilian semi-arid. *Irriga* **2021**, *26*, 490–506. [CrossRef]
29. Stasolla, M.; Neyt, X. Applying Sentinel-1 time series analysis to sugarcane harvest detection. In Proceedings of the IGARSS, Yokohama, Japan, 24 July–2 August 2019; pp. 1–4.
30. Silva, A.S.d.; Moura, G.B.D.A.; Lopes, P.M.O.; Guimarães, M.J.M.; Bezerra, A.C.; Gomes, A.W.A. Predição da produtividade de cana-de-açúcar com base em modelo agrometeorológico no semiárido brasileiro. *Nativa* **2024**, *10*, 515–524. [CrossRef]
31. Araya, S.; Ostendorf, B.; Lyle, G.; Lewis, M. CropPhenology: An R package for extracting crop phenology from time series remotely sensed vegetation index imagery. *Ecol. Inform.* **2018**, *46*, 45–56. [CrossRef]
32. Lange, M.; Doktor, D. phenex: Auxiliary Functions for Phenological Data Analysis, R Package Version 1.4-5. 2017. Available online: https://cran.r-project.org/web/packages/phenex/phenex.pdf (accessed on 5 November 2022).
33. Kong, D.; McVicar, T.R.; Xiao, M.; Zhang, Y.; Peña-Arancibia, J.L.; Filippa, G.; Xie, Y.; Gu, X. phenofit: An R package for extracting vegetation phenology from time series remote sensing. *Methods Ecol. Evol.* **2022**, *13*, 1508–1527. [CrossRef]
34. Forkel, M.; Wutzler, T. *Greenbrown—Land Surface Phenology and Trend Analysis. A Package for the R Software*. Version 2.2. Available online: http://greenbrown.r-forge.r-project.org/ (accessed on 1 March 2023).
35. Digital Earth Australia (DEA). Vegetation Phenology. Available online: https://docs.dea.ga.gov.au/notebooks/Real_world_examples/Vegetation_phenology.html (accessed on 29 June 2024).

36. Jönsson, P.; Eklundh, L. Seasonality extraction by function fitting to time-series of satellite sensor data. *IEEE Trans. Geosci. Remote Sens.* **2002**, *40*, 1824–1832. [CrossRef]
37. Tan, B.; Morisette, J.T.; Wolfe, R.E.; Gao, F.; Ederer, G.A.; Nightingale, J.; Pedelty, J.A. An enhanced TIMESAT algorithm for estimating vegetation phenology metrics from MODIS data. *IEEE J. Sel. Top. Appl. Earth Obs. Remote Sens.* **2011**, *4*, 361–371. [CrossRef]
38. Palmer, S.C.; Odermatt, D.; Hunter, P.D.; Brockmann, C.; Presing, M.; Balzter, H.; Tóth, V.R. Satellite remote sensing of phytoplankton phenology in Lake Balaton using 10 years of MERIS observations. *Remote Sens. Environ.* **2015**, *158*, 441–452. [CrossRef]
39. Kong, D. rTIMESAT: Extract Remote Sensing Vegetation Phenology by TIMESAT Fortran Library. 2021. Available online: https://rdrr.io/github/kongdd/rTIMESAT/ (accessed on 20 June 2024).
40. Rodigheri, G.; Sanches, I.D.; Richetti, J.; Tsukahara, R.Y.; Lawes, R.; Bendini, H.d.N.; Adami, M. Estimating Crop Sowing and Harvesting Dates Using Satellite Vegetation Index: A Comparative Analysis. *Remote Sens.* **2023**, *15*, 5366. [CrossRef]
41. Huete, A.; Didan, K.; Miura, T.; Rodriguez, E.P.; Gao, X.; Ferreira, L.G. Overview of the Radiometric and Biophysical Performance of the MODIS Vegetation Indices. *Remote Sens. Environ.* **2002**, *83*, 195–213. [CrossRef]
42. Myneni, R.B.; Keeling, C.D.; Tucker, C.J.; Asrar, G.; Nemani, R.R. Increased Plant Growth in the Northern High Latitudes from 1981 to 1991. *Nature* **1997**, *386*, 698–702. [CrossRef]
43. Antunes, J.F.G.; Lamparelli, R.A.; De, C.; Rodrigues, L.H.A. Representação de ciclos harmônicos de séries temporais Modis para análise do cultivo da cana-de-açúcar. *Pesqui. Agropecu. Bras.* **2016**, *51*, 1868–1879. [CrossRef]
44. Ramachandra, T.V.; Kumar, U.; Dasgupta, A. *Analysis of Land Surface Temperature and Rainfall with Landscape Dynamics in Western Ghats, India*; Indian Institute of Science: Bangalore, India, 2016.
45. Justice, C.O.; Vermote, E.; Townshend, J.R.G.; Defries, R.; Roy, D.P. The moderate resolution imaging spectroradiometer (MODIS): Land remote sensing for global change research. *IEEE Trans. Geosci. Remote Sens.* **1998**, *36*, 1228–1249. [CrossRef]
46. Hilker, T.; Anderson, M.C.; Masek, J.G.; Wang, P. Fusing Landsat and MODIS Data for Vegetation Monitoring. *IEEE Geosci. Remote Sens. Mag.* **2015**, *3*, 47–60.
47. Xavier, G.d.O.; de Almeida, T.; de Oliveira, C.M.M.; de Oliveira, P.D.S.; Costa, V.H.B.; Granado, L.M.A. Estimate and evaluation of reservoir metrics in Serra da Mesa dam (GO) using the Google Earth Engine platform. *Rev. Ambiente Água* **2020**, *15*. [CrossRef]
48. Jönsson, P.; Eklundh, L. *TIMESAT 3.1—Software Manual*; Lund University: Lund, Sweden, 2004; p. 82. Available online: http://web.nateko.lu.se/timesat/timesat.asp (accessed on 1 May 2021).
49. Jönsson, P.; Eklundh, L. TIMESAT—A program for analyzing time-series of satellite sensor data. *Comput. Geosci.* **2012**, *30*, 833–845. [CrossRef]
50. Eklundh, L.; Jönsson, P. TIMESAT 3.3 with Seasonal Trend Decomposition and Parallel Processing—Software Manual. 2017. Available online: https://web.nateko.lu.se/timesat/docs/TIMESAT33_SoftwareManual.pdf (accessed on 6 July 2024).
51. Jena, S.D.; Poggi, M. Harvest planning in the Brazilian sugar cane industry via mixed integer programming. *Eur. J. Oper. Res.* **2013**, *230*, 374–384. [CrossRef]
52. Usmana, M.; Akramb, N.; Imtiazc, S.; Muneeb, S. Haider Sugarcane: Diseases Due to Pests, Pest Management Strategies and Factors Influencing the Production of Sugarcane. *Am. Sci. Res. J. Eng. Technol. Sci. ASRJETS* **2020**, *65*, 126–139.
53. Ruiz-Ramirez, J.; Hernandez-Rodriguez, G.E.; Zulueta-Rodriguez, R. Time series analysis forecasting in sugar cane production. *Terra Latinoam.* **2011**, *29*, 103–109.
54. Cardozo, N.P.; Sentelhas, P.C. Climatic effects on sugarcane ripening under the infl uence of cultivars and crop age. *Sci. Agric.* **2013**, *70*, 449–456. [CrossRef]
55. Zhao, Y.; Yu, L.X.; Ai, J.; Zhang, Z.F.; Deng, J.; Zhang, Y.B. Climate Variations in the Low-Latitude Plateau Contribute to Different Sugarcane (*Saccharum* spp.) Yields and Sugar Contents in China. *Plants* **2023**, *12*, 2712. [CrossRef] [PubMed]
56. Alvares, C.A.; Stape, J.L.; Sentelhas, P.C.; Moraes, G.J.L.; Sparovek, G. Köppen's climate classification map for Brazil. *Meteorol. Z.* **2013**, *22*, 711–728. [CrossRef]
57. Sampaio, E.V.S.B. Características e potencialidades. In *Uso Sustentável e Conservação dos Recursos Florestais da Caatinga*; Gariglio, M.A., Sampaio, E.V.S.B., Cestaro, L.A., Kageyama, P.Y., Eds.; Serviço Florestal Brasileiro: Brasília, Brazil, 2010; pp. 29–48.
58. Prado, D. As caatingas da América do Sul. In *Ecologia e Conservação da Caatinga*; Leal, I.R., Tabarelli, M., Silva, J.M.C., Eds.; Universitária da UFPE: Recife, Brazil, 2003; pp. 3–73.
59. Nimer, E. Climatologia da região Nordeste do Brasil. Introdução à climatologia dinâmica. *Rev. Bras. Geogr.* **1972**, *34*, 3–51.
60. Sá, P.C.C.d. Estimativa do Saldo de Radiação em Cultivo Irrigado de Cana-de-Açúcar Utilizando Dados de Sensoriamento Remoto Orbital. Master's Thesis, Universidade Federal Rural do Semi-Árido, Mossoró, Brazil, 2016.
61. Cruz, F.N.; Borba, G.L.; Abreu, L.R.D. *Ciências da Natureza e Realidade: Interdisciplinar*; Edufrn: Natal, Brazil, 2005.
62. Medeiros, R.; Andrade, J.; Ramos, D.; Moura, M.; Pérez-Marin, A.M.; dos Santos, C.A.C.; da Silva, B.B.; Cunha, J. Remote Sensing Phenology of the Brazilian Caatinga and Its Environmental Drivers. *Remote Sens.* **2022**, *14*, 2637. [CrossRef]
63. Savitzky, A.; Golay, M.J.E. Smoothing and Differentiation of Data by Simplified Least Squares Procedures. *Anal. Chem.* **1964**, *36*, 1627–1639. [CrossRef]
64. Kong, F.; Li, X.; Wang, H.; Xie, D.; Li, X.; Bai, Y. Land Cover Classification Based on Fused Data from GF-1 and MODIS NDVI Time Series. *Remote Sens.* **2016**, *8*, 741. [CrossRef]

65. Wang, Y.; Zang, S.; Tian, Y. Mapping paddy rice with the random forest algorithm using MODIS and SMAP time series. *Chaos Solitons Fractals* **2020**, *140*, 110116. [CrossRef]
66. Ramírez-Cuesta, J.; Minacapilli, M.; Motisi, A.; Consoli, S.; Intrigliolo, D.; Vanella, D. Characterization of the main land processes occurring in Europe (2000–2018) through a MODIS NDVI seasonal parameter-based procedure. *Sci. Total Environ.* **2021**, *799*, 149346. [CrossRef]
67. Doussoulin-Guzmán, M.A.; Pérez-Porras, F.J.; Triviño-Tarradas, P.; Ríos-Mesa, A.F.; Porras, A.G.F.; Mesas-Carrascosa, F.J. Grassland Phenology Response to Climate Conditions in Biobio, Chile from 2001 to 2020. *Remote Sens.* **2022**, *14*, 475. [CrossRef]
68. Shapiro, S.S.; Wilk, M.B. An analysis of variance test for normality (complete samples). *Biometrika* **1965**, *52*, 591–611. [CrossRef]
69. Kim, T.K. T test as a parametric statistic. *Korean J. Anesthesiol.* **2022**, *68*, 540–546. [CrossRef] [PubMed]
70. QGIS Geographic Information System. Open Source Geospatial Foundation Project. 2024. Available online: http://qgis.osgeo.org (accessed on 15 June 2021).
71. Marcucci, M.; Sharma, S. Applied Multivariate Techniques. *Technometrics* **1997**, *39*, 100–101. [CrossRef]
72. Abdel-Fattah, M.K.; Kotb Abd-Elmabod, S.; Zhang, Z.; Merwad, A.-R.M.A. Exploring the Applicability of Regression Models and Artificial Neural Networks for Calculating Reference Evapotranspiration in Arid Regions. *Sustainability* **2023**, *15*, 15494. [CrossRef]
73. Cohen, J. *Statistical Power Analysis for the Behavioral Sciences*, 2nd ed.; Routledge: New York, NY, USA, 1988. [CrossRef]
74. Willmott, C.J.; Ckleson, S.G.; Davis, R.E. Statistics for the evaluation and comparision of models. *J. Geophys. Res.* **1985**, *90*, 8995–9005. [CrossRef]
75. Camargo, A.P.; Sentelhas, P.C. Avaliação do desempenho de diferentes métodos de estimativa da evapotranspiração potencial no estado de São Paulo, Brasil. *Rev. Bras. Agrometeorol.* **1997**, *5*, 89–97.
76. Bezerra, A.C.; De A. Moura, G.B.; Lopes, P.M.O.; Ribeiro, E.P.; Galvíncio, J.D.; Ferraz, E.X. Como os Produtos MODIS têm sido Utilizados para Análise dos Parâmetros Biofísicos em Regiões Semiáridas? Uma Revisão Bibliométrica e de Literatura. Revista Brasileira de Cartografia. *Rev. Bras. De Cartogr. [S. l.]* **2022**, *74*, 597–615. [CrossRef]
77. Orusa, T.; Viani, A.; Cammareri, D.; Borgogno Mondino, E. A Google Earth Engine Algorithm to Map Phenological Metrics in Mountain Areas Worldwide with Landsat Collection and Sentinel-2. *Geomatics* **2023**, *3*, 221–238. [CrossRef]
78. Huete, A.; Justice, C.O. *MODIS Vegetation Index (MOD 13) Algorithm Theoretical Basis Document*. version 3. Available online: https://modis.gsfc.nasa.gov/data/atbd/atbd_mod13.pdf (accessed on 25 September 2024).
79. Rouse, J.W.; Haas, R.H.; Deering, D.W.; Schell, J.A.; Harlan, J.C. *Monitoring the Vernal Advancement and Retrogradation (Green Wave Effect) of Natural Vegetation*; NASA/GSFC: Greenbelt, MD, USA, 1974.
80. Moreira, M.A. *Fundamentos do Sensoriamento Remoto e Metodologias de Aplicação*, 4th ed.; Universidade Federal de Viçosa: Viçosa, MG, Brazil, 2011; 422p.
81. Soares, J.V.; Batista, G.T.; Shimabukuro, Y.O. Histórico e descrição, Cap1. In *o Sensor MODIS e suas Aplicações Ambientais no Brasil*; Ed. Parênteses: São José dos Campos, Brazil, 2007; 423p.
82. Latorre, M.L.; Shimabukuro, Y.O.; Anderson, L.O. Produtos para ecossistemas terrestres—MODLAND, Cap2. In *o Sensor Modis e suas Aplicações Ambientais no Brasil*; Ed. Parênteses: São José dos Campos, Brazil, 2007; 423p.
83. Hoogenboom, G. Contribution of agrometeorology to the simulation of crop production and its application. *Agric. For. Meteorol.* **2000**, *103*, 137–157. [CrossRef]
84. Pereira, A.R.; Angelocci, L.R.; Sentelhas, P.C. *Agrometeorologia—Fundamentos e Aplicações Práticas*; Ed. Agropecuárial: Guaíba, Brazil, 2002; 478p.
85. Mavi, H.S.; Tupper, G.J. *Agrometeorology—Principles and Application of Climate Studies in Agriculture*; Food Products Press: New York, NY, USA, 2004; 364p.
86. Pinto Santiago, E.J.; Oliveira, G.M.D.; Leitão, M.D.M.V.B.R.; Moura, M.S.B.D.; Gonçalves, I.S. Precipitação esperada, em diferentes níveis de probabilidade, na região de Juazeiro, BA. *J. Environ. Anal. Prog.* **2017**, *2*, 457–464. [CrossRef]
87. Silva, O.; Khramov, D.; Sergieieva, K.; Vasyliev, V. Monitoring of Sugarcane Harvest in Brazil Based on Optical and SAR Data. *Remote Sens.* **2020**, *12*, 4080. [CrossRef]
88. Sentelhas, P.C.; Monteiro, J.E.B.d. Agrometeorologia dos cultivos: Informações para uma agricultura sustentável. In *Agrometeorologia dos Cultivos: o Fator Meteorológico na Produção Agrícola*; Monteiro, J.E.B.A., Ed.; INMET: Brasília, Brazil, 2009; 530p.
89. Bustamante, M.; Nobre, C.; Smeraldi, R.; Aguiar, A.P.; Barioni, L.; Ferreira, L.; de Freitas, L.K.; May, P.; Pinto, A.; Ometto, J. Estimating greenhouse gas emissions from cattle raising in Brazil. *Clim. Chang.* **2012**, *115*, 559–577. [CrossRef]
90. Sentelhas, P.C. *Duração do Período de Molhamento Foliar: Aspectos Operacionais da sua Medida, Variabilidade Espacial em Diferentes Culturas e sua Estimativa a Partir do Modelo de Penman-Monteith*; ESALQ/USP: Piracicaba, Brazil, 2004; 161p.
91. et Larose, M. La canne à sucre. In *Collection Techniques Agricoles et Productions Tropicales*; et Larose, M. Maisonneuve et larose: Paris, France, 1991.
92. Marin, F.R.; Pellegrino, G.Q.; Assad, E.D.; Pinto, H.S.; Zullo Junior, J. Cana de açúcar, Cap7. In *Agrometeorologia dos Cultivos: O Fator Meteorológico na Produção Agrícola*; Monteiro, J.E.B.A., Ed.; INMET: Brasília, Brazil, 2009; 530p.
93. Suguitani, C. *Entendendo O Crescimento E Produção da Cana-de-Açúcar: Avaliação do Modelo Mosicas. TESE (Doutorado em Agronomia)—Escola Superior de Agricultura Luiz de Queiroz*; Universidade de São Paulo: Piracicaba, Brazil, 2006.
94. Santos, J.M.; Lopes, P.M.O.; Moura, G.B.A.; Slva, A.S.; Silva, J.L.B.; Oliveira Junior, J.G. Análise de canaviais irrigados com parâmetros biofísicos por sensoriamento remoto no Nordeste Brasileiro. *Rev. Irrig.* **2021**, *26*, 638–663. [CrossRef]

95. Dotaniya, M.L.; Datta, S.C.; Biswas, D.R.; Dotaniya, C.K.; Meena, B.L.; Rajendiran, S.; Regar, K.L.; Lata, M. Use of sugarcane industrial by-products for improving sugarcane productivity and soil health. *Int. J. Recycl. Org. Waste Agric.* **2016**, *5*, 185–194. [CrossRef]
96. Soares, J.M.; de S. Vieira, V.J.; Gomes Junior, W.F.; de Araújo Filho, A.A. Agrovale: Uma experiência de 25 anos em Irrigação da Cana-de-açúcar na região do Submédio São Francisco. *Rev. ITEM* **2003**, *60*, 5–62.
97. Carvalho, H.F.S.; Moura, M.S.B.; Leitão, M.M.V.B.R.; Rodrigues, C.T.A.; Da Silva, T.G.F. Albedo de Caatinga Preservada Comparado com Cultivo de Cana-De-Açúcar Irrigada. In Anais do XX Congresso Brasileiro de Agrometeorologia, Embrapa. Juazeiro: Brazil, 2017.
98. Souza, A.M.; Santos e Silva, C.M.; Bezerra, B.G. Albedo da Caatinga preservada e substituída por pastagem no Nordeste do Brasil. *Atmosfera* **2021**, *12*, 1622.
99. Gunnula, W.; Kosittrakun, M.; Righetti, T.L.; Weerathaworn, P.; Prabpan, M. Normalized difference vegetation index relationships with rainfall patterns and yield in small plantings of rain-fed sugarcane. *Aust. J. Crop Sci.* **2011**, *5*, 1845–1851.
100. Aguiar, D.A.D.; Silva, W.F.; Rizzi, R.; Rudorff, B.F.T.; Sugawara, L.M.; Paes, L.A.D. Monitoramento da colheita da cana. In *O Sensor Modis E Suas Aplicações Ambientais No Brasil*; Rudorff, B.F.T., Shimabukuro, Y.E., Ceballos, J.C., Eds.; Bookimage: São José dos Campos, Brazil, 2007; pp. 123–131.
101. Ceddia, M.B.; Anjos LH, C.D.; Lima, E.; Ravelli Neto, A.; Silva, L.A.D. Sistemas de colheita da cana-de-açúcar e alterações nas propriedades físicas de um solo Podzólico Amarelo no Estado do Espírito Santo. *Pesqui. Agropecu. Bras. Brasília* **1999**, *34*, 1467–1473. [CrossRef]
102. Rede Interuniversitária para o Desenvolvimento do Setor Sucroenergético (RIDESA). Catálogo Nacional de Variedades "RB" de Cana-de-Açúcar, Curitiba: Rede Interuniversitária Para o Desenvolvimento do Setor Sucroalcooleiro. *Curitiba.* 2010. Available online: https://www.ridesa.com.br/ (accessed on 21 September 2022).
103. CONAB (Companhia Nacional de Abastecimento). Acompanhamento da Safra Brasileira de Cana-de-Açúcar, Safra 2018/19—Segundo Levantamento, Brasília, Brazil. 2018, 2020. Available online: https://www.conab.gov.br/info-agro/safras/cana (accessed on 27 April 2024).
104. Baghdadi, N.; Cresson, R.; Todoroff, P.; Moinet, S. Multitemporal Observations of Sugarcane by TerraSAR-X Images. *Sensors* **2010**, *10*, 8899–8919. [CrossRef]
105. Lisboa, I.P.; Damian, J.M.; Cherubin, M.R.; Barros, P.P.S.; Fiorio, P.R.; Cerri, C.C.; Cerri, C.E.P. Prediction of Sugarcane Yield Based on NDVI and Concentration of Leaf-Tissue Nutrients in Fields Managed with Straw Removal. *Agronomy* **2018**, *8*, 196. [CrossRef]
106. Oré, G.; Alcântara, M.S.; Góes, J.A.; Teruel, B.; Oliveira, L.P.; Yepes, J.; Castro, V.; Bins, L.S.; Castro, F.; Luebeck, D.; et al. Predicting Sugarcane Harvest Date and Productivity with a Drone-Borne Tri-Band SAR. *Remote Sens.* **2022**, *14*, 1734. [CrossRef]

Disclaimer/Publisher's Note: The statements, opinions and data contained in all publications are solely those of the individual author(s) and contributor(s) and not of MDPI and/or the editor(s). MDPI and/or the editor(s) disclaim responsibility for any injury to people or property resulting from any ideas, methods, instructions or products referred to in the content.